applied sciences

IMPACT FACTOR 2.5

CITESCORE 5.3

Review

Numerical Simulation of an Optical Resonator for the Generation of Radial Laguerre–Gauss LG_{p0} Modes

Kamel Aït-Ameur, Michael Fromager and Abdelkrim Hasnaoui

MDPI

https://doi.org/10.3390/app15063331

applied sciences

MDPI

Review

Numerical Simulation of an Optical Resonator for the Generation of Radial Laguerre–Gauss LG_{p0} Modes

Kamel Aït-Ameur [1,*], Michael Fromager [1] and Abdelkrim Hasnaoui [2]

[1] Centre de Recherche sur les Ions, les Matériaux et la Photonique (CIMAP), UMR6252 CEA-CNRS-ENSICAEN-Université de Caen, 6 Bd. Maréchal Juin, F14050 Caen CEDEX 4, France; michael.fromager@ensicaen.fr

[2] Institut National d'Optométrie d'Ouled Fayet (INOOF), Résidence les Palmiers, Ouled Fayet, Algiers RW233, Algeria; hasnaouikrimo@yahoo.fr

* Correspondence: kamel.aitameur@ensicaen.fr

Abstract: The research on high-order transverse modes in lasers is a subject as old as the laser itself and has been largely abandoned. However, recently several studies have demonstrated an interest in using, instead of the usual Gaussian beam, a radial Laguerre–Gauss LG_{p0} beam, as, for instance, one can observe a strong improvement, for a given power, in the longitudinal and radial forces in optical tweezers illuminated by a LG_{p0} beam instead of the usual Gaussian beam. Since in most commercial lasers, the delivered laser beam is Gaussian, we therefore think it opportune to consider the problems of forcing a laser to oscillate individually on a higher-order transverse LG_{p0} mode. We propose a comprehensive analysis of the effects of an intra-cavity phase or amplitude mask on the fundamental mode of a plano-concave cavity. In particular, we discuss the best choice of parameters favouring the fundamental mode of a pure radial Laguerre–Gauss LG_{p0} model.

Keywords: intra-cavity beam shaping; high-order Laguerre–Gauss modes; binary amplitude mask; binary phase mask

Received: 4 February 2025
Revised: 12 March 2025
Accepted: 13 March 2025
Published: 18 March 2025

Citation: Aït-Ameur, K.; Fromager, M.; Hasnaoui, A. Numerical Simulation of an Optical Resonator for the Generation of Radial Laguerre–Gauss LG_{p0} Modes. *Appl. Sci.* **2025**, *15*, 3331. https://doi.org/10.3390/app15063331

1. Introduction

Research on high-order transverse modes of laser cavities was mainly conducted by early pioneers after the invention of the laser in 1960 [1–6] and was very quickly abandoned. It should be noted, however, that a renewed interest in the study of high-order transverse modes of lasers which can be found, without being exhaustive, in references [7–11]. The high-order transverse modes involve Hermite (Laguerre) polynomials for rectangular (cylindrical) coordinates. In the following text, we will emphasise radial Laguerre–Gauss LG_{p0} modes. The mathematical description of the high-order transverse mode is available in the standard textbooks in photonics [12–14]. The electric field associated with a LG_{p0} beam is given by

$$\begin{aligned} E_p(\rho,z) &= E_0 \frac{W_0}{W(z)} L_p\left(\frac{2\rho^2}{W^2(z)}\right) \times \exp\left(-\frac{\rho^2}{W^2(z)}\right) \\ &\times \exp\left(i(2p+1)\Phi(z) - \frac{ik\rho^2}{2R_c(z)}\right) \end{aligned} \quad (1)$$

where ρ and z are the radial and longitudinal coordinates, respectively, and L_p is the Laguerre polynomial of order p [15]. The quantities W and R_c are the width of the Gaussian

mode ($p = 0$), and the wavefront radius of curvature, respectively, are z-dependent as well as the Gouy phase shift Φ:

$$W^2(z) = W_0^2\left[1 + \left(\frac{z}{z_R}\right)^2\right] \tag{2}$$

$$R_c(z) = z\left[1 + \left(\frac{z_R}{z}\right)^2\right] \tag{3}$$

$$\Phi(z) = Arctg\left(\frac{z}{z_R}\right) \tag{4}$$

The LG_{p0} beams are made of a central peak surrounded by p rings of light as shown in Figure 1.

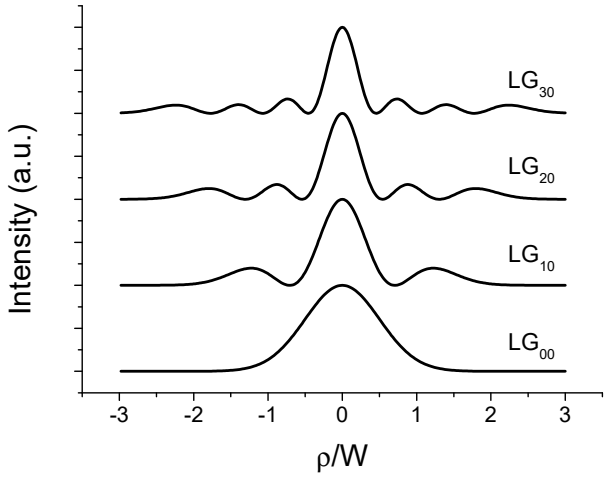

Figure 1. Transverse intensity distribution of the 4-first radial Laguerre–Gauss LG_{p0} beams.

The Gaussian LG_{00} beam is characterised by its beam-waist radius W_0 and a Rayleigh distance of $z_R = \pi W_0^2/\lambda$. The beam waist plane defines the origin $z = 0$ of the longitudinal coordinate. The lateral spreading of the LG_{p0} beams are described by the width W_p, based on the second moment radius, and the far-field angular divergence θ_p, given by [16]:

$$W_p(z) = W(z)\sqrt{2p+1} \tag{5}$$

$$\theta_p = \theta_0\sqrt{2p+1} \tag{6}$$

where $\theta_0 = \lambda/(\pi W_0)$ is the angular divergence of the Gaussian beam ($p = 0$). Another important property of LG_{p0} beams is that they have the same on-axis ($\rho = 0$) intensity whatever the mode order p. This contrasts with the usual scale law stating that beam spreading results in a decrease in the on-axis intensity as the beam propagates [17]. Another quantity of importance that characterises the beam quality, called the beam propagation factor, was popularised by A.E. Siegman [18,19] and is equal to $M^2 = (2p+1)$ for an LG_{p0} beam. This enables us to introduce a fundamental quantity known as brightness, B [16]

$$B = \frac{\pi^2 P}{\lambda^2 (M^2)^2} \tag{7}$$

The brightness B describes the potential of a laser beam carrying a power P and with a beam propagation factor M^2 in order to realise high intensities in combination with a large Rayleigh range. Note that a beam with a beam propagation factor of equal to one is Gaussian but the reverse is not true [19,20]. Equation (7) allows us to understand why the studies of higher-order transverse modes slowed after the invention of the laser, on the

pretext that only the Gaussian LG_{00} mode is useful because of its higher brightness over the higher-order LG_{p0} beam. The consequence of this rejection is that most of commercial lasers still deliver a Gaussian beam (GB). However, recent laser studies on higher-order transverse modes have demonstrated numerous advantages in several laser applications. Recently, a review about the advantages and disadvantages of using structured LG_{p0} beams for certain applications (3D microfabrication, optical tweezers, spherical aberration mitigation) was published [21]. In addition to this, there are numerous studies on the applications of LG_{p0} beams in the gravitational wave detectors [22–26]. First of all, let us clarify the concept of fundamental mode of a laser cavity since it is often confused in the literature with the Gaussian mode. The fundamental mode of a laser cavity is the mode with the lowest losses and is thus susceptible to reaching the laser oscillation first.

The objective of this paper is to present a model (see Appendix A) of a laser cavity, including a phase or amplitude mask aiming to force the fundamental mode of the laser cavity to become a pure LG_{p0} beam. "Pure" means that the mode is a single mode, i.e., not a mix of several transverse modes. The amplitude and phase masks impose the position of zeros of the intensity of the desired LG_{p0} mode. The amplitude mask takes the form of thin annular absorbing rings with a radius which follows closely the location of the Laguerre polynomial zeros given in Table 1 for the three first high-order LG_{p0} modes. For convenience and clarity, we limited ourselves to $p = 3$, but it may be perfectly feasible to achieve a laser oscillation on higher-order transverse modes when forced by a binary amplitude or phase mask.

Table 1. Values of ratio ρ_i/W such that $L_p(2\rho_i^2/W^2) = 0$.

p			
1	0.707106		
2	0.541195	1.306562	
3	0.455946	1.071046	1.773407

The use of absorbing rings for forcing a LG_{p0} mode has been already attempted [27]. For instance, Hermite–Gauss modes have been obtained by inserting straight wires inside a laser cavity aligned along the nodes of the desired mode [28,29]. In Section 2, we will consider the selection of a transverse LG_{p0} mode based on the insertion of a binary amplitude mask inside the cavity, which induced high losses in all modes except the specific desired mode.

The second way that masks are able to force laser oscillation in LG_{p0} mode is through a phase mask, and more precisely, a binary phase mask, which is made up of a transparent material etched on annular zones and introduces a phase shift equal to 0 or π and consequently a transmittance equal to +1 or -1. The radii of the phase discontinuities are (0 to π), and (π to 0) corresponds to the node radii of the LG_{p0} mode given in Table 1. In the following text, the phase mask will be known as a binary annular phase plate (BAPP), and it will be shown in Section 3 that, for the amplitude mask, the mechanism of transverse mode selection differs from that mentioned above. It is important to note that, for several decades, the selection of the fundamental mode of a laser cavity consisted of suppressing all high-order transverse modes except the Gaussian LG_{00} mode by inserting a circular aperture into the resonator [1,2,4,30–34]. In this case, the selected LG_{00} mode is distorted by the diffraction and is no longer Gaussian in shape, as shown theoretically and experimentally [35]. Note that the selection of the fundamental LG_{00} mode by the circular internal

aperture is based on the hierarchy of beam divergence of the LG_{p0} modes expressed, in accordance with Equation (6), by the inequalities

$$\theta_0 < \theta_1 < \theta_2 < \theta_3 \ldots \tag{8}$$

By adjusting the diaphragm opening, it is possible to select the mode with the smallest divergence. In Section 3, it will be shown that the binary phase mask known as the circular phase plate (CPP) is able to change the hierarchy divergence so that the fundamental mode selected by the internal aperture is a high-order LG_{p0} mode. There are some experimental works on lasers oscillating in a high-order transverse mode selected with the help of a binary phase mask [36–38]. For the generation of very high-order Laguerre–Gauss modes, there is the possibility of inserting a spherical aberration inside the cavity [39–42]. The latter will not be addressed here, and we will focus exclusively on the use of binary amplitude or phase masks.

As mentioned above, in Sections 2 and 3, we will detail the action on a LG_{p0} beam of two elementary components, which are the bases of the amplitude and phase masks. These basic components are the absorbing ring and the circular phase discontinuity ($0 \rightarrow \pi$) known as the circular phase plate (CPP). The resulting effects of these masks on a LG_{p0} beam are directly induced losses (for amplitude masks) and the modification of beam divergence hierarchy of the LG_{p0} base (for the phase mask). In general, we will search for the best conditions for each mask to obtain a fundamental mode, i.e., a pure LG_{p0} beam. Appendix A illustrates the mathematical development of the numerical model which allows the determination of the resonant field of an optical cavity, including a diaphragm and a binary mask.

2. Single-Pass and Multi-Pass Properties of Binary Amplitude Masks

Our aim is to determine the fundamental mode of a laser cavity containing an amplitude or phase mask in accordance with the following methodology. The latter consists of considering, first, the single-pass diffraction properties, for instance losses and angular divergence, of the mask when illuminated by a LG_{p0} beam. In the second step, we consider the mask properties resulting from multi-pass diffraction which occur when the mask is inserted inside a resonant cavity. The single-pass properties help us to understand the multi-pass properties of the mask inserted inside a cavity.

2.1. Absorbing Ring: Single-Pass Properties

The geometry of the considered absorbing ring of interest is shown in Figure 2. The first property of the opaque ring illuminated by a LG_{p0} beam to be considered is its transmission, labelled as T_p, defined as the ratio of transmitted and incident powers:

$$T_p = \frac{\int_0^{\rho_A} I_p(\rho)\rho d\rho + \int_{\rho_B}^{\infty} I_p(\rho)\rho d\rho}{\int_0^{\infty} I_p(\rho)\rho d\rho} \tag{9}$$

where $I_p(\rho) = \left|E_p(\rho)\right|^2$ is the intensity distribution of the incident LG_{p0} beam. The losses introduced by the ring are equal to $L_p = (1 - T_p)$ and are shown in Figure 3a as a function of the normalised ring radius at $\Delta = 20$ µm.

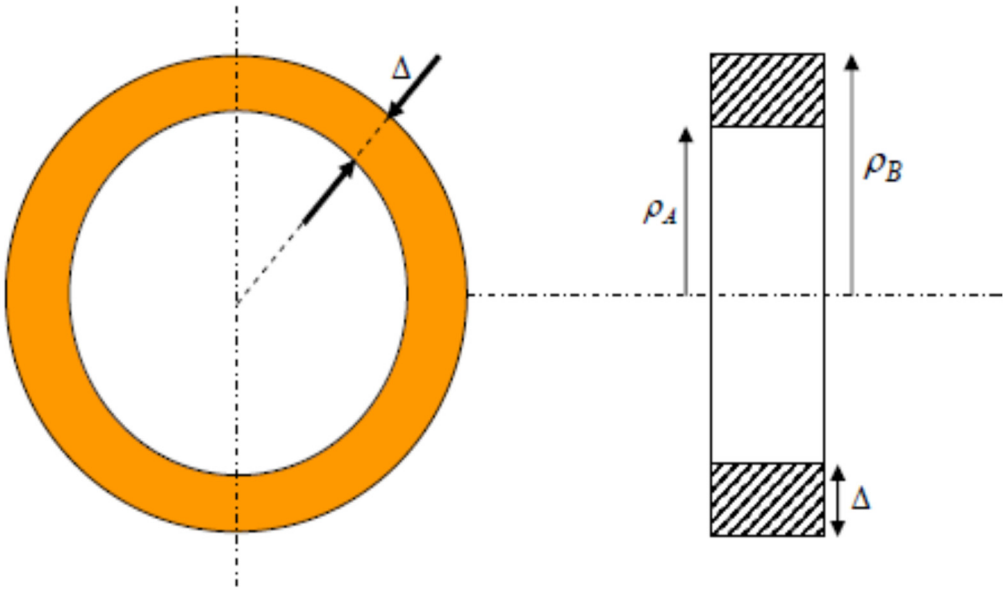

Figure 2. Absorbing ring of internal (external) radius $\rho_A(\rho_B)$ and of width Δ.

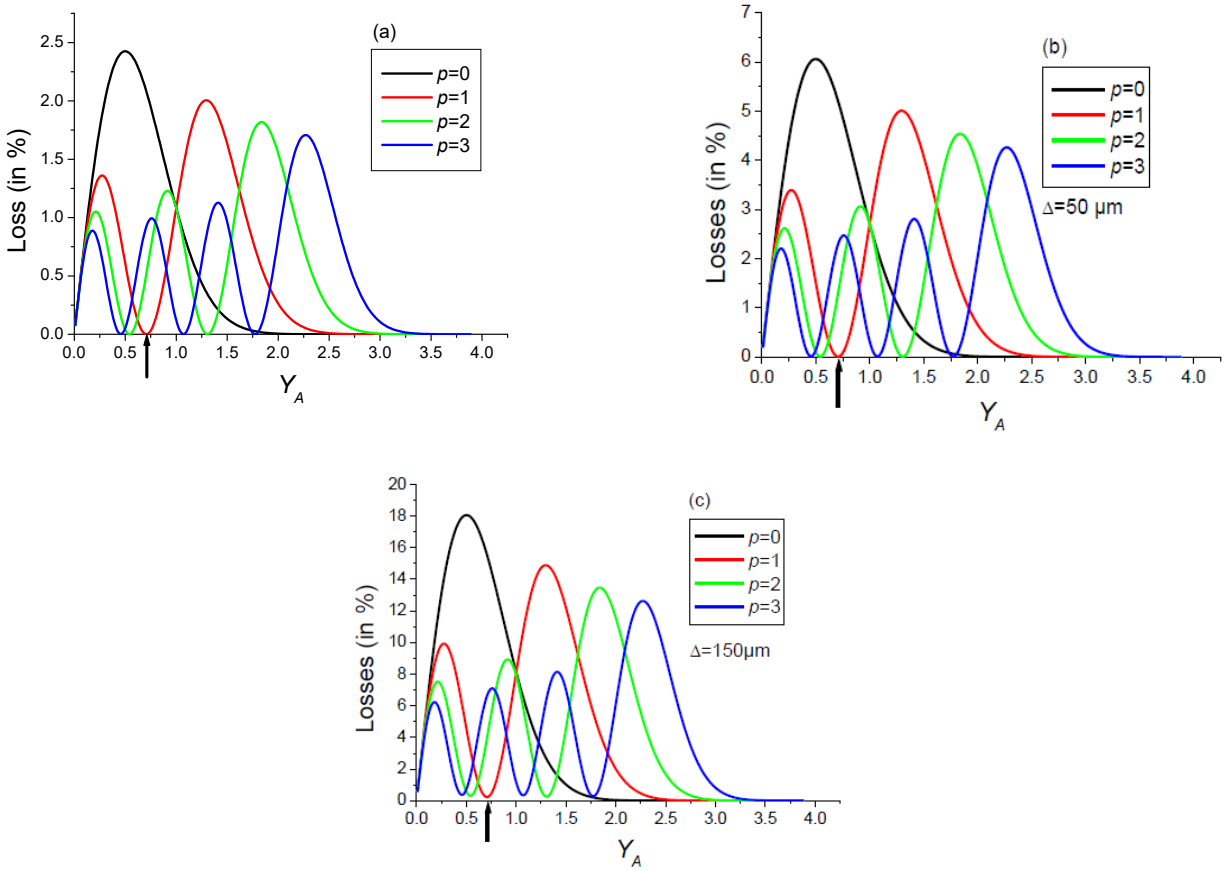

Figure 3. Variations in the losses $L_p = (1 - T_p)$ introduced by an absorbing ring versus the normalised radius $Y_A = \rho_A / W$. The incident light is a symmetrical Laguerre–Gauss LG_{p0} beam of the order p. The lowest-order LG_{00} beam has a width W = 1 mm. The ring width is (**a**) 20 μm, (**b**) 50 μm, (**c**) 150 μm.

In Figure 3a, it can be seen that the hierarchy formed by the set of losses (L_0, L_1, L_2, and L_3) changes as the ring diameter changes. In particular, one can observe that the losses introduced by the ring have a minimum value very close to zero whenever the ring is positioned on a node of intensity while the other modes suffer higher losses. This results in interesting modal properties when the absorbing ring is inserted inside a cavity as will be

discussed later. In order demonstrate that a thin absorbing ring positioned on a LG_{p0} node results in low losses, in Table 2, we outlined the minima of L_p.

Table 2. Minimum value of losses L_p when a ring of width Δ = 20 μm is set on the successive nodes.

Zero#	1	2	3
$(L_1)_{\min}$ in %	0.002		
$(L_2)_{\min}$ in %	7.5×10^{-4}	6.2×10^{-4}	
$(L_3)_{\min}$ in %	0.0016	9.4×10^{-4}	6.7×10^{-4}

Usually, the fundamental mode TEM_{00} (transverse electromagnetic) of the cavity is a Laguerre–Gauss LG_{00} mode (cylindrical symmetry) or a Hermite–Gauss HG_{00} (rectangular symmetry), i.e., a Gaussian beam. However, if an opaque ring is introduced inside the resonator, then the fundamental mode TEM_{00} of the cavity could be a high-order transverse LG_{p0} mode, since it is the mode with the lowest losses. This is why it is pertinent to talk about a fundamental mode, which is a high-order transverse mode depending on the inserted filter or mask, introducing high losses to all transverse modes except the desired LG_{p0} mode, which suffers the lowest losses. Since the hierarchy of divergence given in Equation (8) plays an important role in the transverse mode discrimination, we need to verify if the ring is able or unable to change the hierarchy of divergence. However, we will begin by considering the influence of the ring width Δ on the loss hierarchy. The plots in Figure 3b,c of losses L_p for Δ = 50 μm (Δ = 150 μm) versus the normalised ring radius shows that the curves exhibit similar profiles except that one obtains higher losses when increasing the ring width Δ.

Hereafter, we will determine the fundamental mode, i.e., the mode with the lowest losses, of a plano-concave cavity, including a circular diaphragm and an opaque ring. It is clear that, if we aim for instance for a LG_{10} mode, then it would be judicious to set the size of the ring so that $Y_A = 0.707$, which corresponds to the LG_{10} node, as shown by the arrow in Figure 3a–c. However, the ring will have succeeded in overcoming the other transverse modes, but given the losses due to the diaphragm this will not favour them. This is why it is important to examine the variations in the far-field angular divergence θ_p of the LG_{p0} beam diffracted by the amplitude ring. The results are shown in Figure 4a,b for Δ = 20 μm (Δ = 150 μm). In order to determine whether the absorbing ring is able to change the divergence hierarchy, we will calculate the angular divergence θ_p of the diffracted LG_{p0} beam upon the ring as follows:

$$\theta_p = \frac{W_e}{D} \tag{10}$$

where the effective width W_e, determined in the far-field at a distance D = 30 m, is based on the second moment [43] of the diffracted intensity distribution $I_d(r, D)$ in plane $z = D$:

$$W_e^2 = \frac{2\int_0^\infty I_d(r,D) r^3 dr}{\int_0^\infty I_d(r,D) r dr} \tag{11}$$

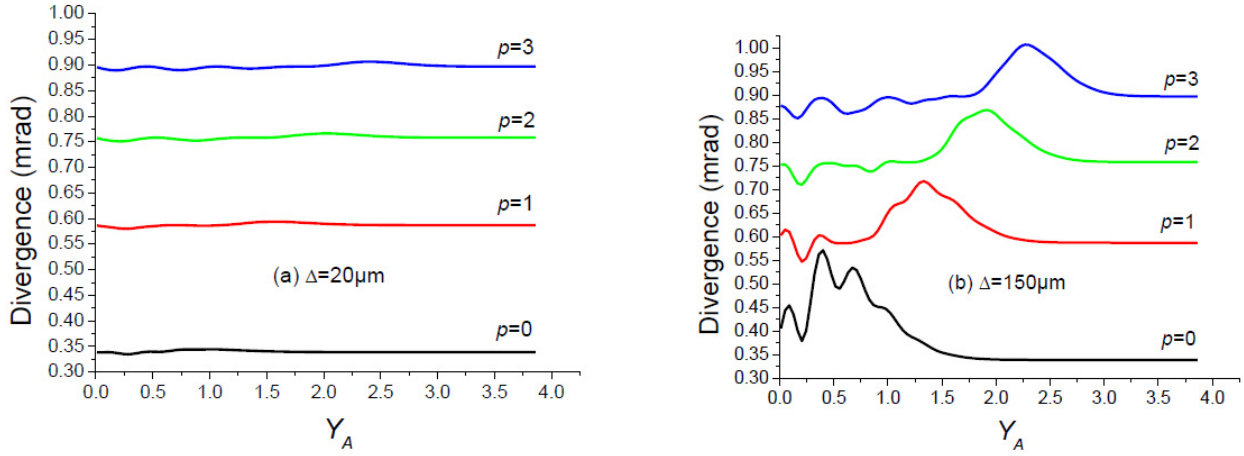

Figure 4. Variations in the LG_{p0} beam divergence diffracted by an opaque ring of width (**a**) Δ = 20 μm and (**b**) Δ = 150 μm versus its normalised radius $Y_A = \rho_A / W$.

The transverse intensity distribution $I_d(r, D) = |E_d(r, z = D)|^2$ is obtained from the diffracted electric field $E_d(r, z)$, expressed by the well-known Fresnel–Kirchhoff integral:

$$E_d(r,z) = \frac{2\pi}{\lambda z}\int_0^{\infty} \tau_R(\rho) E_p(\rho) \exp\left[\frac{-i\pi\rho^2}{z\lambda}\right] J_0\left[\frac{2\pi}{\lambda z} r.\rho\right] \rho d\rho \tag{12}$$

where J_0 is the zero-order Bessel function of first order. r (ρ) is the radial coordinate ob the plane z (ring). The calculation of Equation (12) is carried out with the help of a FORTRAN code based on the numerical integrator *dqdag* from the International Mathematics and Statistical Library (IMSL). The quantity $\tau_R(\rho)$ defines the opaque ring transmission:

$$\tau_R(\rho) = \begin{cases} 0 & \text{for } \rho_A \le \rho \le \rho_B \\ +1 & \text{elsewhere} \end{cases} \tag{13}$$

Figure 4a shows that the ring with a width Δ = 20 μm does not change the hierarchy of divergence expressed by Equation (8), but, as shown in the plot in Figure 4b, when Δ = 150 μm, the beam divergence is highly impacted so that, for instance, θ_0 and θ_1 move very close to, i.e., the node of LG_{10}. As a consequence of the fundamental mode of the cavity, including an opaque ring ($Y_A = 0.707$), initially desired to be a LG_{10} mode, could potentially be a LG_{00} mode. Consequently, it would be wise to use a narrow width opaque ring unless a cavity without a selecting diaphragm is envisaged. The single-pass properties of the opaque ring suggest that positioning the ring inside a cavity on a node of a given LG_{p0} mode would enable the laser oscillation on the chosen LG_{p0} mode. However, this could occur only if the other modes are subject to higher losses, thus preventing their oscillation. As it will be shown later, this issue of the oscillation locking onto a single high-order transverse mode can be addressed by considering the transverse mode discrimination expressed as the ratio of losses associated with two neighbouring modes in terms of losses. Here, we can extent this concept to the single-pass properties of the ring by considering the ratio of losses, such as L_0/L_1, L_2/L_1, and L_3/L_1 in a situation when, for instance, the desired mode is LG_{10}. The plots in Figure 5a show $Y_A = 0.707$ (LG_{10} node), where the opaque ring efficiently identifies the undesired modes, i.e., the LG_{00}, LG_{20}, and LG_{30} modes. Consequently, the ring set inside a laser cavity could force the laser oscillation onto the LG_{10}, since the losses for the other modes are greater than those of L_1.

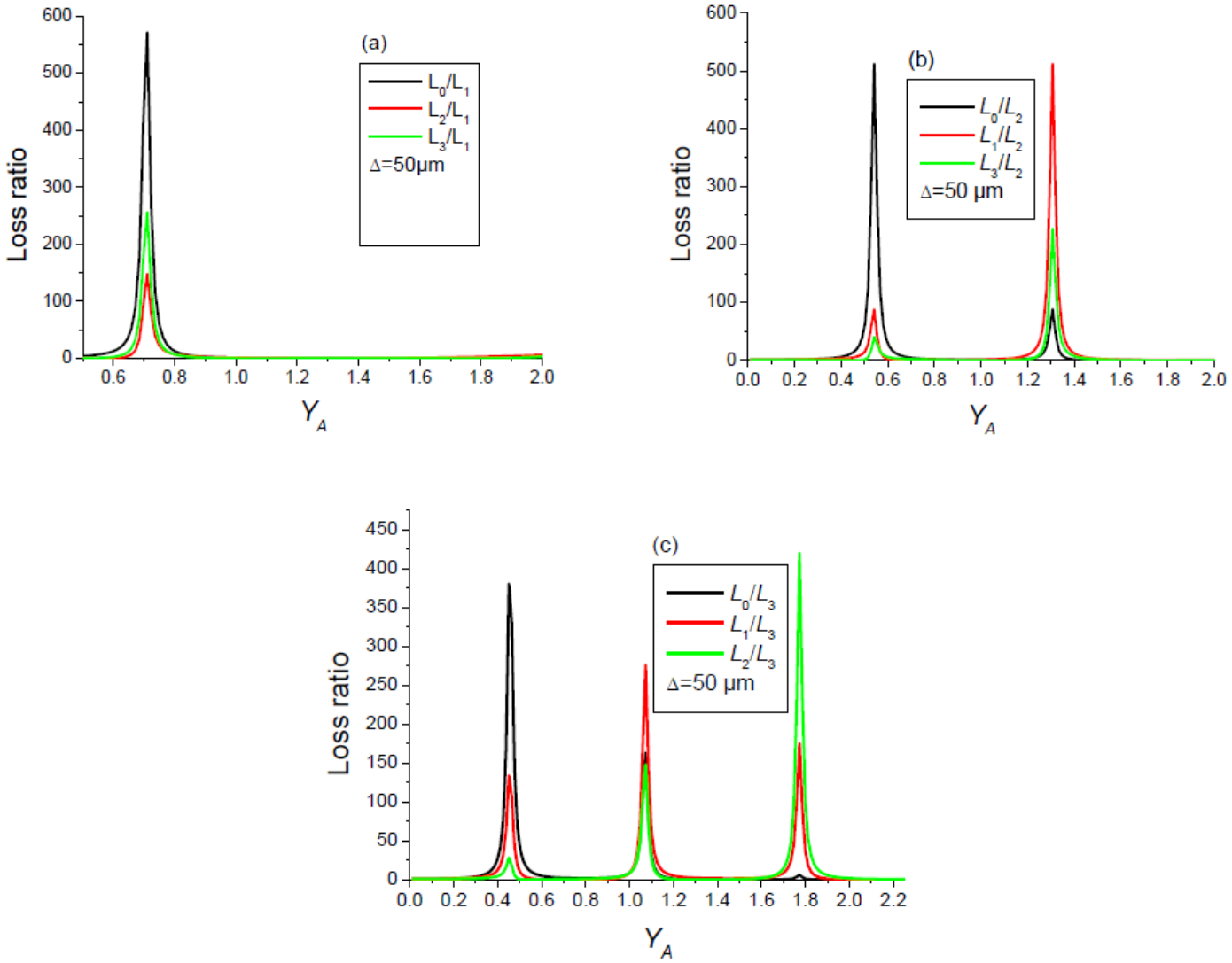

Figure 5. Variations in the loss ratios as a function of Y_A, the normalised ring radius.

The same reasoning can be applied to the LG_{20} mode by considering the variations in the loss ratios L_0/L_2, L_1/L_2, and L_3/L_2, as functions of Y_A, and the normalised ring radius. Similarly to the LG_{20} mode, it can be that the loss ratios L_0/L_2, L_1/L_2, and L_3/L_2 display a pair of peaks when Y_A is varied, and results are shown in Figure 5b. These two peaks are centred on the two LG_{20} nodes, i.e., $Y_A = 0.54$ and $Y_A = 1.3$. Forcing a laser cavity to oscillate on a single-high-order transverse mode clearly results in the difficulty of averting the risk of the oscillation of the Gaussian LG_{00} mode. In terms of this, when enabling the LG_{20} mode, the plots in Figure 5b suggest that the ideal position of the opaque ring is on the first node, i.e., $Y_A = 0.54$. When considering the oscillation of the LG_{10} mode, however, the situation is quite the opposite, since setting the ring on the second node allows a better discrimination against the LG_{10} mode. Let us now perform the same analysis concerning the LG_{30} mode.

Figure 5c represents the variations in the loss ratios L_0/L_2, L_1/L_2, and L_3/L_2 and logically presents three peaks centred on the three nodes of the desired LG_{30} mode, i.e., $Y_A = 0.45$, 1.07, and 1.77. It can be seen that setting the ring on the first (third) node, results in the bad discrimination of the LG_{20} (LG_{00}) mode, since the loss ratio L_2/L_3 (L_0/L_3) is low. Finally, in order to favour the LG_{30} mode, the second node ($Y_A = 1.07$) seems to be the best position for setting the opaque ring, since the undesired modes (p = 0, 1, and 2) are well discriminated against.

Now, it is important to check whether there is the possibility of improving the discrimination of undesired transverse modes by introducing a second opaque ring in order to favour the LG_{20} mode. The first step of the study is the calculation of the losses introduced by the two rings shown in Figure 6. Figure 7 shows the variations in the losses L_p introduced by the twin absorbing ring as a function of Y_A while maintaining the ratio Y_C/Y_A at a value 2.41, which represents the ratio of the position of the two LG_{20} node positions, i.e., 2.41 = 1.3065/0.5411.

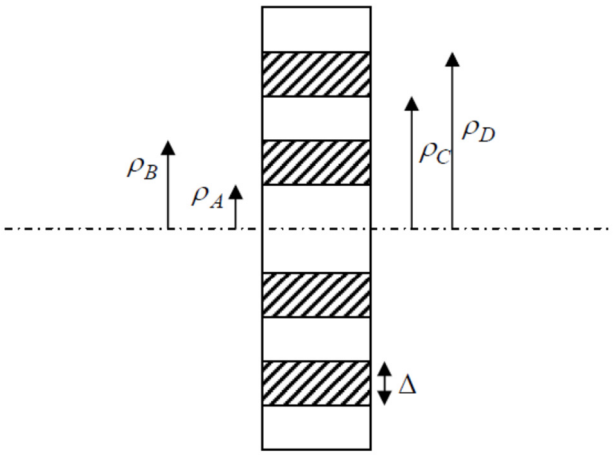

Figure 6. Scheme of the twin absorbing ring characterised by four normalised radii $Y_A = \rho_A/W$, $Y_B = (\rho_B/W) = Y_A + \Delta/W$, $Y_C = \rho_C/W$, and $Y_D = (\rho_D/W) = Y_C + \Delta/W$. The width of the rings is Δ = 50 µm.

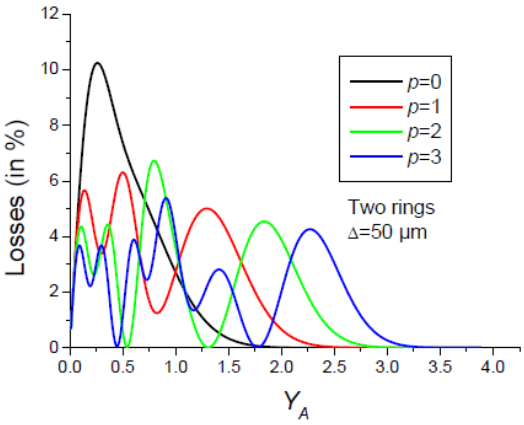

Figure 7. Variations in the losses $L_p = (1 - T_p)$ introduced by two absorbing rings versus the normalised radius $Y_A = \rho_A/W$. The incident light is a symmetrical Laguerre–Gauss LG_{p0} beam of order p. The lowest order LG_{00} beam has a width W = 1 mm.

In Figure 7, it can be seen that the LG_{10} beam losses are significantly increased compared to the losses shown in Figure 4, and then an improvement of the discrimination is expected. To confirm this, the loss ratio variations in Figure 8 are investigated. The first peak corresponds to the twin ring positioned on the two nodes of the LG_{20} beam. It is clear that compared to the plots in Figure 5b, the presence of the second absorbing ring greatly improved the discrimination against the LG_{10} and LG_{30} beams. However, nothing changed for the second peak centred on $Y_A = 1.30$ since the second absorbing ring positioned at $Y_C = 1.30 \times 2.41 = 3.13$ is outside the lateral extent of the LG_{20} beam.

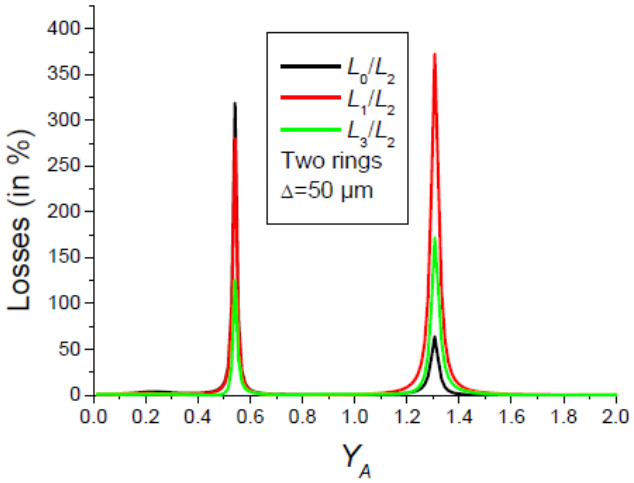

Figure 8. Variations in the loss ratios L_0/L_2, L_1/L_2, and L_3/L_2 as a function of the normalised first ring radius. The width of the each ring is Δ = 50 μm.

2.2. Multi-Pass Properties of Absorbing Rings

The resonator considered here is plano-concave cavity of length L and is made up of a plane mirror and a concave mirror with a radius of the curvature as R. Figures A1 and A2 (see Appendix A) show the cavity, including an absorbing ring or a CPP or BAPP on the concave mirror side, and a circular diaphragm on the plane mirror. The method used for the determination of the resonant field is based on its decomposition via Laguerre–Gauss functions (see Appendix A). Moreover, the diaphragm and the absorbing ring or the binary phase mask can be switched. Both situations will be addressed below. On one hand, the sensitivity of the beam width on mirrors with thermal lensing is different, and consequently, so is the "detuning" of the targeted zero of the expected LG_{p0} mode. On the other hand, this provides a verification for the method which forces the fundamental mode to be a LG_{p0} mode whatever the relative position of the selecting diaphragm and the diffracting object (ring or phase mask). Before proceeding, it is useful to note two geometric parameters of interest which characterise the Gaussian mode of the bare cavity, i.e., without the diaphragm or other diffracting object, namely, the Gaussian mode radius W_p (W_c) on the plane (concave) mirror:

$$W_p^2 = \frac{\lambda L}{\pi}\left(\frac{g}{1-g}\right)^{1/2} \tag{14}$$

$$W_c^2 = W_p^2/g \tag{15}$$

where the cavity geometric parameter $g = (1 - L/R)$ is kept in the stable region ($0 < g < 1$) by varying R, the radius of the curvature of the concave mirror. In the case where the amplifying medium is set in front of the concave mirror, the effect of the thermal lensing can be accounted for through a variable effective radius of curvature. The variations in W_p and W_c versus parameter g are shown in Figure 9a, and their derivatives are shown in Figure 9b. Note that g = 0.5 is a remarkable value since the derivative dW_c/dg is null, and the consequence is that the best position of the diffracting object (ring or phase mask) should be near the concave mirror so as to avoid the phenomena of the transverse mode flip due to a variable thermal lens.

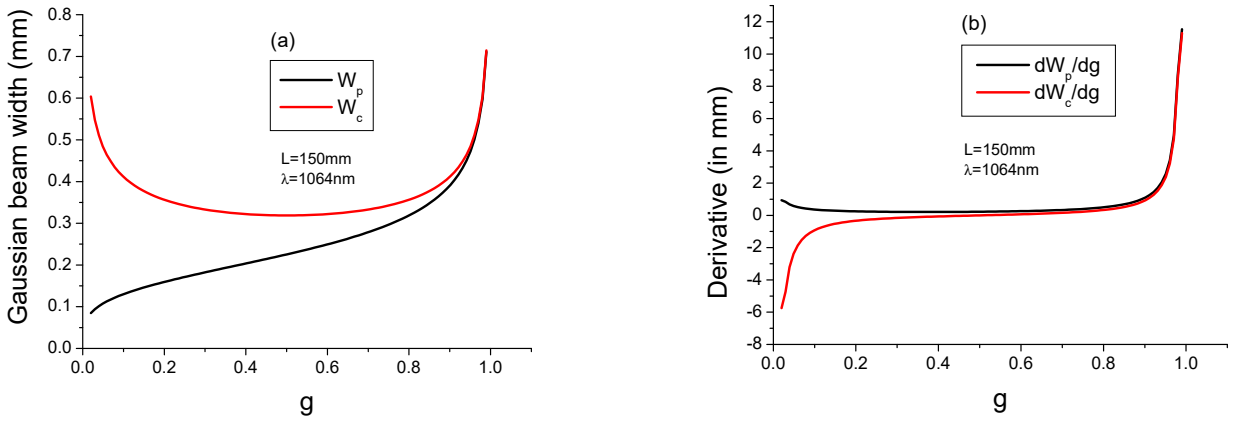

Figure 9. (**a**) Gaussian mode radius W_p (W_c) on the plane (concave) mirror versus the geometric parameter g. (**b**) Gaussian mode derivative radius dW_p/dg (dW_c/dg) versus the geometric parameter g.

Three quantities (see Appendix A) are calculated in order to characterise the fundamental mode of the cavity, including an absorbing ring and a diaphragm: L_{FM} is the fundamental mode losses, F_c is the transverse mode discrimination, and M^2 is the propagation factor of the output beam. The latter allows us to identify the type of LG_{p0} beam, which is susceptible to oscillate, as shown in equation $M^2 = (2p + 1)$, corresponding to a pure LG_{p0} beam.

Since the absorbing ring may only impose one single zero, we are interested in a fundamental mode; specifically, a LG_{10} mode since it has one node. It will be shown later that the absorbing ring inside the resonator can impose a fundamental mode, which can be a higher-mode order ($p \geq 2$). Let us first examine an important point concerning the positioning of the ring relative to the dark ring of the desired LG_{10} mode. Indeed, when the ring has a certain width Δ, it is crucial to pay attention to the overlap of the target node which has to be at its middle. In the next section, we will use the ratio $Y_R = (Y_A + Y_B)/2$, which is associated with the normalised radius of the central part of the absorbing ring. In the following text, we will confirm whether a single absorbing ring is able to impose a LG_{p0} mode as the fundamental mode of a cavity of length L. An absorbing ring with a fixed radius $\rho_R = (\rho_A + \rho_B)/2$ = 180 µm is inserted inside the cavity, as shown in Figure A2. The ratio $Y_R = (Y_A + Y_B)/2 = \rho_R/W_c$ is varied by changing the geometrical parameter $g = (1 - L/R)$ by adjusting the cavity length. The ratio Y_R is set as equal to the first zero of the three first LG_{p0} modes (p = 1, 2, and 3) and the normalised diaphragm radius noted Y_c is adjusted so that the fundamental mode loss L_{FM} is the same for the different values of Y_R, insofar as is possible. The results are shown in Table 3, which displays the cavity length L, Y_R, Y_c, L_{FM}, the transverse mode discrimination F_c, and the M^2 factor of the beam emerging from the plane mirror. All these parameters are defined in the Appendix A.

Table 3. Loss L_{FM} of the fundamental mode, which can be LG_{10}-, LG_{20}-, or LG_{30}-like in shape, depending on Y_R, the normalised radius of the ring. The width of the ring is Δ = 20 µm.

L (mm)	g	Y_R	Y_c	L_{FM} in %	F_c	M^2	Figure 10
93	0.38	0.707	3.9	0.25	5.9	3.005	a
124	0.17	0.54	4.1	0.2	10	5	b
137	0.08	0.45	3.4	0.2	3	7.008	c

The transverse intensity profiles of the cavity fundamental mode, selected with the parameters given in Table 3, in the far-field region (z = 10 m) are shown in Figure 10 (blue curves). The plots in red colour represent the intensity distributions of the pure LG_{p0} beam.

One can note that the fundamental mode in Figure 10a is very close to the perfect LG_{10} mode, while it slightly moves away from a pure LG_{p0} beam as p increases, although not very much.

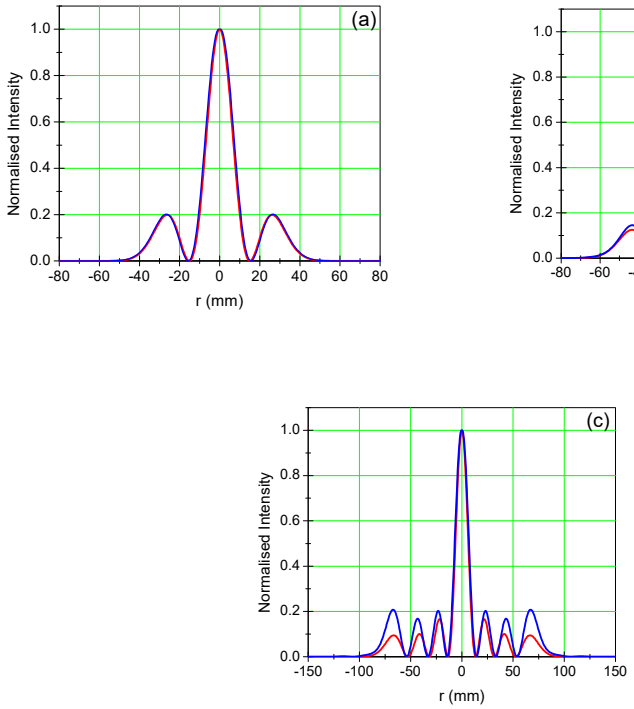

Figure 10. The plots in blue colour represent the transverse intensity distribution of the cavity fundamental mode. The calculations have been made up for the parameters of Table 3 in the far-field region at a distance z = 10 m from the cavity of Figure A2 (out#1). The plots in red colour correspond to a pure LG_{p0} mode. (**a**) L = 93 mm, (**b**) L = 124 mm, and (**c**) L = 137 mm.

At this point, the opaque ring is set against the plane mirror and the diaphragm is set close to the concave mirror, playing the role of output (Figure 11). This configuration of cavity is very close to an experiment setup used to control the transverse mode of a solid-state laser using an amplitude mask made up of concentric absorbing rings [27]. The characteristics of the cavity are as follows: L = 260 mm; R = 300 mm; λ = 1064 nm; g = 0.133; and W_p = 186 μm.

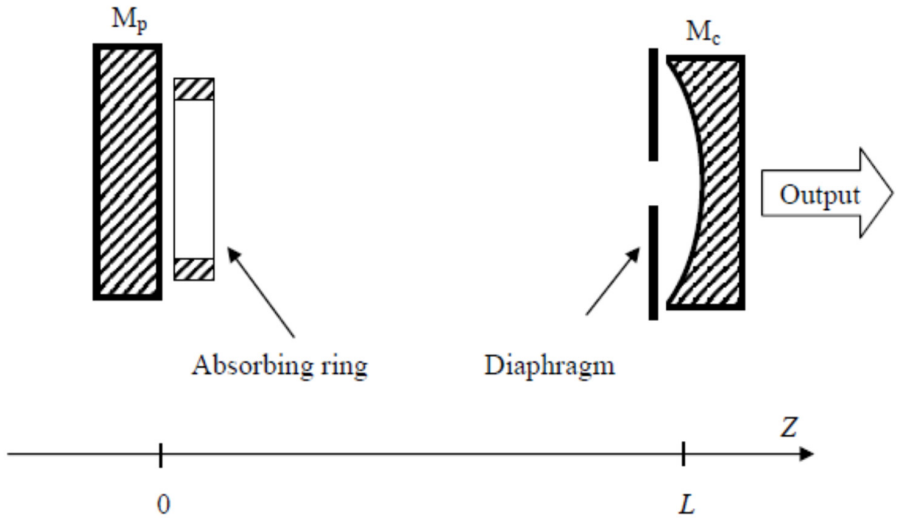

Figure 11. Scheme of the plano-concave cavity, including an amplitude mask on the plane mirror and a circular diaphragm on the output concave mirror of radius of curvature, R = 300 mm. The cavity length

is constant and equal to L = 277 mm. This cavity configuration is close to that used in the experiment [27], and the parameters are as follows: L = 260 mm; R = 300 mm; λ = 1064 nm; g = 0.133; W_p = 186 μm.

Before considering the cavity shown in Figure 11, which contains an amplitude mask set against the plane mirror and is made up of one, two, or three absorbing rings, we will examine the role of the presence or the absence of the diaphragm on the selection of a LG_{p0} mode with one absorbing ring. For this study, we considered a cavity with different parameters: L = 600 mm; g = 0.5; λ = 1064 nm; and W_p = 0.45 mm. Initially, we chose this half-confocal configuration (g = 0.5) because it corresponds to the maximum of the transverse mode discrimination [44]. In order to force the laser cavity to exhibit the fundamental mode, i.e., an LG_{p0} mode, it is not sufficient to set the opaque ring on one of the zeros of the polynomial L_p. Indeed, doing that would in principle introduce more losses to the other modes than the desired LG_{p0} mode, as shown in Figure 3. However, as is shown in Figure 4a, the hierarchy of mode divergence is not disturbed by the presence of the absorbing thin ring. Consequently, the losses introduced by the diaphragm could be in competition with the action of the ring so that the fundamental mode could remain the usual Gaussian beam with $M^2 = 1$. This is confirmed by the plot in Figure 12, which displays a flip in the M^2 factor value when the diaphragm radius is changed. Consequently, positioning the absorbing ring on a node is not sufficient for forcing the fundamental mode to be a high-order transverse LG_{p0} mode. We must be aware of any clipping effect that could favour the Gaussian LG_{00} mode. On the other hand, in the absence of a diaphragm, the selection of a particular LG_{p0} mode can be compromised by the phenomenon of transverse mode jump. Indeed, in order to be concrete, let us consider an absorbing ring of width Δ = 20 μm set against the plane mirror (Figure 11), intended to impose the first dark ring of the LG_{20} mode. The cavity has a beam waist radius of W_p = 0.45 mm. As a consequence, the normalised radius of the ring is characterised by $Y_R = 0.54$, $Y_A = Y_R - \Delta/(2W_p) = 0.51$, and $Y_A = Y_R + \Delta/(2W_p) = 0.56$. In Figure 13, we observe, effectively, a fundamental mode, i.e., an LG_{20} mode, confirmed by the propagation factor $M^2 \approx 5$ and characterised by very a low loss $L_{FM} = 0.1\%$. However, if the beam waist radius W_p suffers a variation of about 6.6% for any reason (thermal lensing, cavity length change), such that the normalised ring radius becomes $Y_R = 0.57$ ($Y_A = 0.546$, $Y_B = 0.593$), then the selected mode is a high-order transverse mode with p = 11, since its second zero is $(\rho/W_p) = 0.57$. Thus, to avoid the phenomenon of transverse mode jump when selecting a high-order transverse LG_{p0} mode, two precautions must be taken, i.e., a sufficiently small ring width Δ and an intra-cavity diaphragm for reducing high losses to the undesired higher-order transverse modes. Instead of the intra-cavity diaphragm, the same result can be obtained by limiting the radial size of the pumped region in the amplifying medium. Another possibility for avoiding the transverse mode jumping is to use an amplitude mask made up of concentric absorbing rings positioned on each node of the desired LG_{p0} mode, as shown in Figure 14.

Now, let us consider the performance of the cavity shown in Figure 11 with the parameters L = 260 mm; R = 300 mm; λ = 1064 nm; g = 0.133; and W_p = 186 μm, as well as an amplitude mask, as shown in Figure 14, made up of one, two, or three absorbing rings that coincide, respectively, with the nodes of the modes LG_{10}, LG_{20}, and LG_{30}. The radii of the rings are given in Table 4.

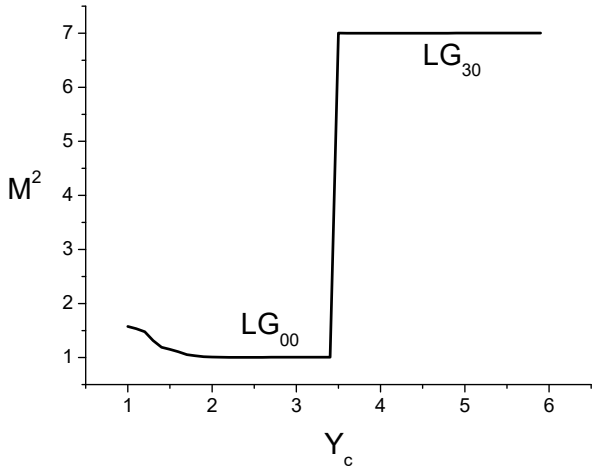

Figure 12. The cavity configuration is shown in Figure 10c The plot shows the variation in the output M^2 factor versus Y_c, the normalised diaphragm radius, when the opaque ring of width Δ = 20 μm is set on the third zero ($Y_R = 1.77$) of the LG_{30} mode.

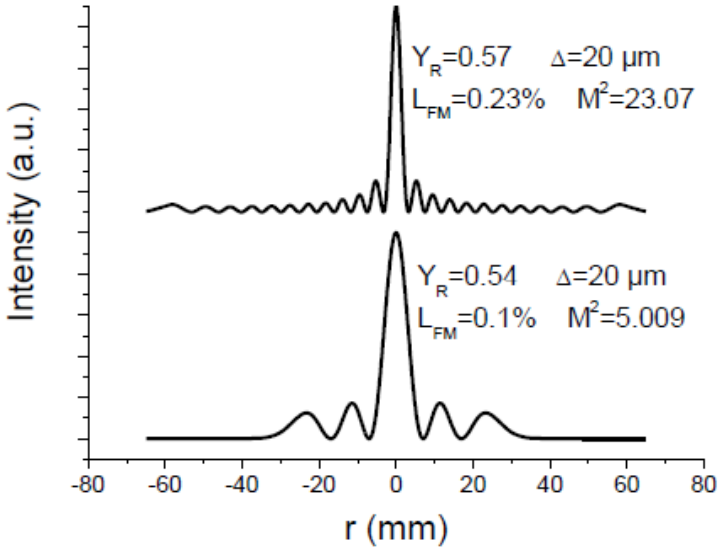

Figure 13. Far-field pattern of the fundamental mode of the cavity, including the plane mirror, an absorbing ring characterised by a normalised radius, Y_R.

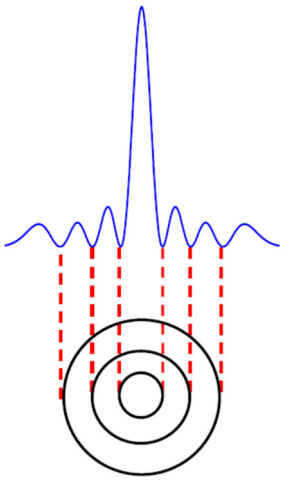

Figure 14. Amplitude mask made up of opaque rings coinciding with the zeros of intensity of the desired LG_{p0} mode, for instance, an LG_{30} mode.

Table 4. Sizes of the absorbing rings, which correlate to the amplitude masks with one (p = 1), two (p = 2), or three rings (p = 3).

p	Radius of the Rings in µm		
1	131		
2	100	243	
3	85	199	330

In the following section, we will provide the parameters that characterise the transverse mode selection (L_{FM}, M^2, and F_c) for a selecting mask made up of one, two, or three absorbing rings with a variable width Δ. The results are given in Table 5 (one ring), Table 6 (two rings), and Table 7 (three rings).

Table 5. Amplitude mask with one absorbing ring, intended to yield the LG_{10} mode with a propagation factor $M^2 = 3$.

Δ (µm)	Y_c	ρ_c (mm)	M^2	L_{FM}	F_c
10	1.65	0.84	1.08	11.5%	1.63
10	2.5	1.3	3.018	0.25%	53
15	1.65	0.84	1.09	16.25%	1.42
15	2.5	1.3	3.02	0.4%	23.6
20	1.65	0.84	1.07	20.7%	1.34
20	2.5	1.3	3.008	0.87%	11.35
25	1.65	0.84	1.1	25%	1.14
25	2.5	1.3	3.008	1.7%	9.4

Table 6. Amplitude mask with two absorbing rings, intended to yield the LG_{20} mode with a propagation factor $M^2 = 5$.

Δ (µm)	Y_c	ρ_c (mm)	M^2	L_{FM}	F_c
10	2	1.02	1.03	14.5%	1.9
10	3	1.53	5	0.3%	28.4
15	2	1.02	1.03	20.5%	1.15
15	3	1.53	5	0.8%	19
20	2	1.02	1.012	26.2%	1.05
20	3	1.53	5.01	1.9%	9.2
25	2	1.03	1.03	31.7%	1.15
25	3	1.53	5	3.4%	1.28

Table 7. Amplitude mask with three absorbing rings, intended to yield the LG_{30} mode with a propagation factor $M^2 = 7$.

Δ (µm)	Y_c	ρ_c (mm)	M^2	L_{FM}	F_c
10	2	1.02	1.016	17%	1.23
10	3.5	1.78	7	0.4%	23.6
15	2	1.02	1.016	24%	1.12
15	3.5	1.78	7	1.5%	10
20	2	1.02	1.016	31%	1.08
20	3.5	1.78	7	3.2%	5.6
25	2	1.02	1.016	37.5%	1.05
25	3.5	1.78	7	5.7%	1.08

The following aspects can be extracted from Tables 5–7:

- The selection of a pure high-order transverse LG_{p0} mode by an amplitude mask made up of p absorbing rings positioned on the nodes of the desired mode works well provided that the diaphragm is sufficiently open. Otherwise, the fundamental mode becomes the Gaussian mode with $M^2 = 1$.
- The losses of the fundamental mode LG_{p0} increase with the width Δ of the absorbing rings.
- The transverse mode discrimination of the cavity decreases with the increase in Δ.

The main conclusion is that it is preferable to use absorbing rings with a small width in order to ensure low losses and a high transverse mode discrimination and to prevent the overlapping of several nodes, leading to a mixing of high-order transverse modes. Note that the intra-cavity generation of selected Laguerre–Gaussian modes of variable radial order, from 0 to 5, has been demonstrated experimentally [27]. The major disadvantage of this method of transverse mode selection is that the selecting mask is enables loss and is questionable for use in a high-power laser, even though the rings are set in beam regions where the intensity is relatively weak. As a consequence, in the next section, a binary phase mask, which is fundamentally transparent and does not possess Fresnel reflections, is used to reach the same objectives. For high-power solid-state laser systems operating on a fundamental mode, a high-order transverse mode imposed by an intra-cavity amplitude or a phase mask, one of the major problems is the thermal effects, which could introduce a certain instability in the mode order through a change in the beam size with pumping power. However, there are several solutions for compensating the thermally induced lens, and these are described in detail in the literature [45–50].

3. Single-Pass and Multi-Pass Properties of a Binary Phase Mask

3.1. Single-Pass Properties of a Binary Phase Mask

As mentioned previously, it is possible to force the laser cavity into the fundamental mode, which is an LG_{p0} mode, by imposing the zeros of intensity by inserting a binary phase mask made up of a transparent material on which is etched a relied, as this gives rise to annular zones which introduce a phase shift equal to 0 or π and create a transmittance equal to +1 or -1. The radii of phase discontinuities ($0 \rightarrow \pi$) and ($\pi \rightarrow 0$) correspond to the node radii of the desired LG_{p0} mode, as shown in Table 1. At the position of these phase discontinuities, the electric field passes from a positive to a negative value, and thus, it is necessarily zero at that position. Note that the binary diffractive optical elements constitute a family of diffractive devices, which are the simplest diffractive components to fabricate since they require only one level of etching. Binary diffractive optics have been used very extensively for beam shaping in various wavelength fields (terahertz, infrared, visible, and X-rays) for a very long time [51–58]. Following a methodology similar to the one used for the amplitude mask, it will be shown below that the mechanism of transverse mode selection differs from that mentioned above for the binary amplitude mask. The annular phase mask (BAPP) described above is made up of several "elementary bricks". This elementary brick consists of a CPP made up of a circular phase discontinuity of radius R_{PI} described by Equation (A14). Obviously, the CPP does not attenuate the incident LG_{p0} beam since it is transparent. However, the hierarchy of divergence associated with each LG_{p0} beam is no longer described by the inequality given by Equation (8). In fact, we will use the same method implemented for the absorbing ring when calculating the angular divergence of the beam passing through the CPP not once, but twice, as shown in Figure 14 The reasons justifying this double-pass are given in the Appendix A.

Figure 15 shows the set-up considered for determining the variations of the LG_{p0} beam passing twice through the CPP. The results are shown in Figure 16, which illustrates the variations in the divergence of the LG_{p0} versus the normalised CPP radius $Y_{PI} = R_{PI}/W_0$,

where W_0 is the width of the incident Gaussian term. It can be seen in Figure 16 that the beam has the smallest divergence (indicated by arrows *A*, *B*, and *C*) and can be either the LG_{30}, LG_{20}, or LG_{10} beam, depending on R_{PI} the CPP radius. A closer look shows that these minima occur when R_{PI} corresponds to the first zero of intensity of the incident LG_{p0} beam. More generally, the divergence is also minimum when the CPP radius corresponds to any zero of the LG_{p0} beam.

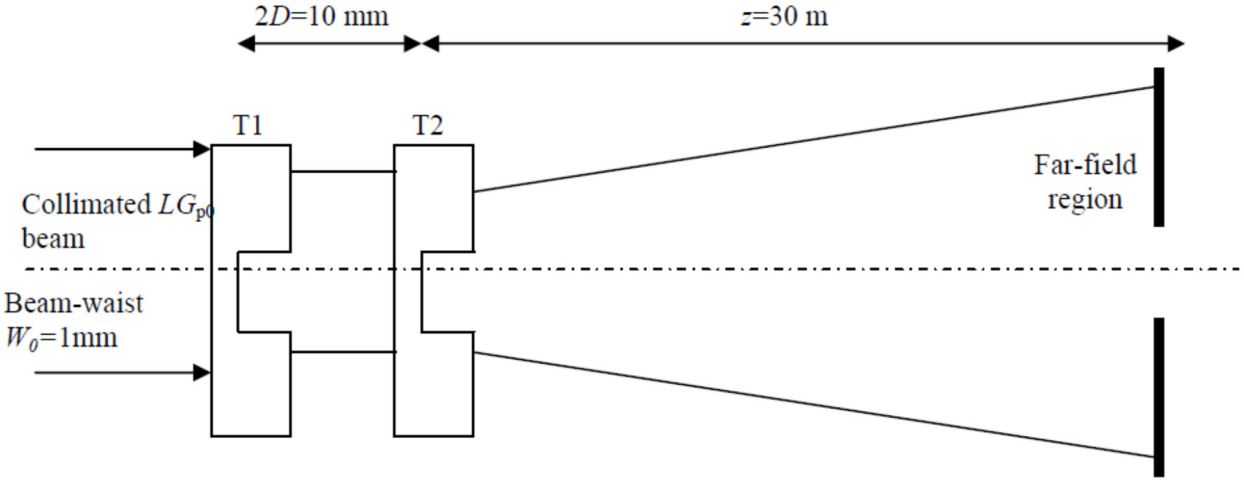

Figure 15. Apparatus allowing to determine the diffracting properties of the cascade of two circular phase plates (CPP) separated by a distance $2D$ = 10 mm. The diffracted field is determined in the far-field at a distance z = 30 m by using Equation (12).

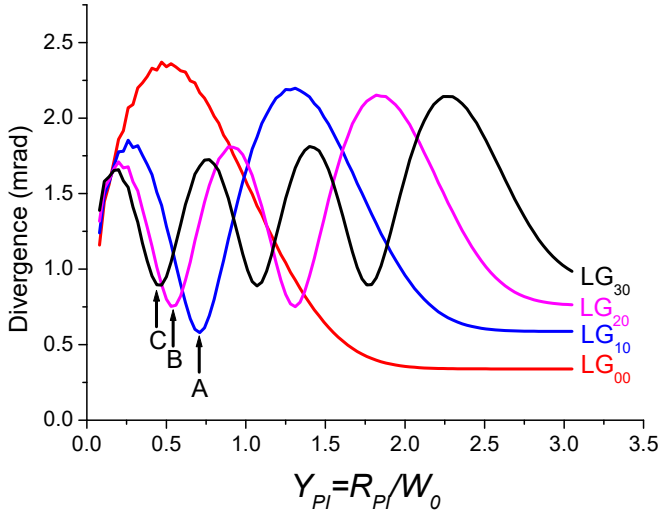

Figure 16. Variations in the divergence $\theta_e = W_e/z$, calculated by using Equations (11) and (12), of the diffracted LG_{00}, LG_{10}, LG_{20}, and LG_{30} beams passing twice through the CPPs versus Y_{PI}, the normalised CPP radius. The arrows A, B, and C indicate the smallest divergence of the LG_{10}, LG_{20}, LG_{30}, respectively.

If we combine the CPP with a diaphragm set in its far-field, as shown in Figure 15, then it would be possible to install a hierarchy of losses susceptible to favouring the transmission of any LG_{p0} beam for adequate R_{PI} and diaphragm radius R_D. For convenience, we introduce the normalised diaphragm radius $Y_D = R_D/W_z$, where W_z would be the width of the LG_{00} beam in the diaphragm plane, i.e., at a distance of z = 30 m. The variations in the losses introduced by the diaphragm versus Y_{PI} were determined for two values of the normalised diaphragm radius, $Y_D = 3.5$ (Figure 17a) and $Y_D = 6.5$ (Figure 17b). It can be seen in Figure 17a that a diaphragm that is not open enough does not allow the instigation of the fundamental mode in a cavity, as shown in Figure A2, but could result

in a high-order transverse mode by setting the phase discontinuity of the CPP on the first node of the desired LG_{p0} mode. However, for a diaphragm that is wide open ($Y_D = 6.5$), as is seen in Figure 17b, a hierarchy of losses takes place which is similar to that shown in Figure 16. The latter allows the possible oscillation of a LG_{p0} mode, provided the value of Y_{PI} is adjusted for minimizing the losses. It has been demonstrated experimentally [59] that a CPP set inside a solid-state laser cavity is able to impose the fundamental mode, which is an LG_{p0} mode (p = 1, 2, 3).

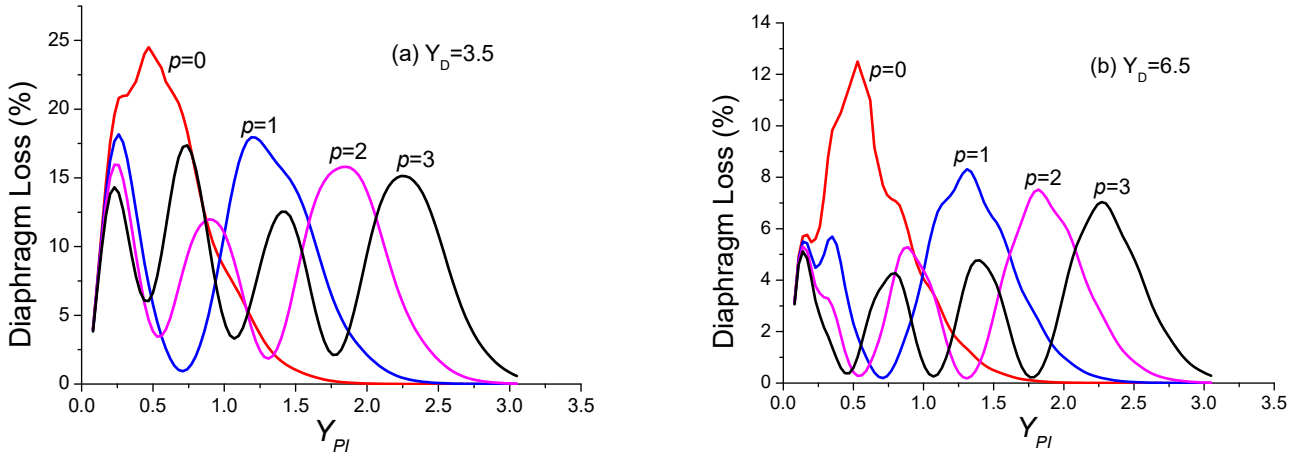

Figure 17. Variations in the losses of the diaphragm set at a distance of z = 30 m versus $Y_{PI} = R_{PI}/W$ for (**a**) $Y_D = 3.5$ and (**b**) $Y_D = 6.5$. The beam incident on the cascade of the CPP is a LG_{p0} beam whose Gaussian term has a width of W_0 = 1 mm.

The discrimination property of the CPP is related to the value of the divergence of the other modes rather than the one targeted by the phase circle discontinuity of the CPP. Table 8 shows that the greater the divergence difference, the more discrimination is expected.

Table 8. Particular values of the divergence of diffracted LG_{p0} (p = 0, 1, 2, and 3) beams passing twice through the CPP shown in Figure 15. The circle phase discontinuity is set on the first node of the incident LG_{p0} beam. The minimum divergence is indicated in red.

Y_{PI}	θ_0 (rad)	θ_1 (rad)	θ_2 (rad)	θ_3 (rad)
0.707	22.6×10^{-4}	6.1×10^{-4}	12.4×10^{-4}	16.4×10^{-4}
0.541	23.5×10^{-4}	10.9×10^{-4}	7.5×10^{-4}	11×10^{-4}
0.455	23×10^{-4}	14.6×10^{-4}	10×10^{-4}	8.9×10^{-4}

It is also interesting to estimate the expected transverse mode discrimination by considering the losses introduced by a diaphragm with a normalised radius equal to $Y_D = 6.5$ and located at a distance z = 30m from the cascade of the two CPP. The results are shown in Table 9, which also contains the discrimination factor F_c, defined as the inverse ratio of the two first losses. In the next section, we will confirm whether the use of a BAPP, setting a phase circle discontinuity on all nodes of the desired LG_{p0} mode, improves or does not improve the transverse mode discrimination factor F_c.

Now, it remains for us to study the single-pass properties of the binary annular phase plate (BAPP) with geometry described by Equation (A15) and by Figure 18, which represents the transmittance profile $\tau_{DOE}(\rho)$ of the considered BAPP. The phase discontinuities circles of the BAPP correspond to the zeros of intensity given in Table 1.

Table 9. Variations in losses induced by the diaphragm of normalised radius $Y_D = 6.5$ set at a distance $z = 30$ m from the cascade of the two CPP. F_c is the discrimination factor defined as the inverse ratio of the two first losses. The minimum in the loss value is indicated in red.

Y_{PI}	Loss for $p = 0$	Loss for $p = 1$	Loss for $p = 2$	Loss for $p = 3$	F_c
0.707	7.7%	0.19%	2.13%	3.95%	11.2
0.541	9.38%	1.64%	0.26%	1.2%	4.6
0.455	8.9%	3.33%	0.95%	0.35%	2.7

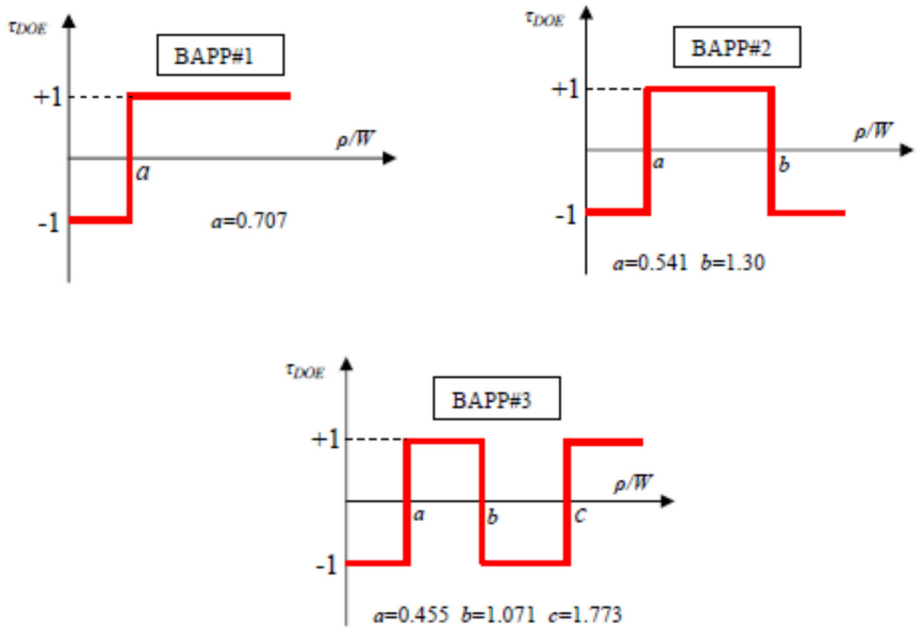

Figure 18. Transmittance profile (field ratio) of the BAPP#p intended to select a LG_{p0} when inserted in the cavity shown in Figure A1.

As performed previously for the CPP, we will consider the properties of the BAPP#p given in Figure 18 through the losses (Table 10) induced on a LG_{p0} beam passing through a cascade of two BAPP#p, as a result of a diaphragm set in the far-field at a distance $z = 30$ m.

Table 10. Variations in losses induced by the diaphragm of normalised radius $Y_D = 6.5$ set at a distance $z = 30$ m from the cascade of the two BAPP. F_c is the discrimination factor defined as the inverse ratio of the two first losses. The minimum in the loss value is indicated in red.

BAPP	Loss for $p = 0$	Loss for $p = 1$	Loss for $p = 2$	Loss for $p = 3$	F_c
#1	7.7%	0.19%	2.13%	3.95%	11.2
#2	10.67%	10.74%	0.48%	4.92%	10.25
#3	15.2%	10.98%	11%	0.65%	16.9

A comparison between Tables 9 and 10 indicates a transverse mode discrimination improvement forthe BAPP compared to the CPP. The question of high-transverse mode discrimination is very important from a practical point of view, since it allows the laser to oscillate on a single high-order transverse mode with a large range of pumping power. In the next section, we will consider the fundamental mode of a laser cavity in which a CPP or a BAPP is inserted.

3.2. Multi-Pass Properties of a Binary Phase Mask

First, we will consider the fundamental mode of the cavity previously shown in Figure A1, with the parameters given in Table 3, in which a CPP with its phase discontinuity

positioned on the first node of LG_{p0} modes (p = 1, 2, and 3) is inserted. The results are summarised in Table 11. The fundamental mode can be either a LG_{00}, LG_{10}, or LG_{20} mode, but with a low transverse mode discrimination. These results are in a good agreement with a previous experiment [59]. It is worth mentioning that the opening or closing of the diaphragm does not allow any transverse mode jumps, as shown above in Figures 12 and 13. Indeed, whatever the diaphragm opening, it is the mode with the smallest divergence which undergoes the lowest losses. The hierarchy of losses is imposed by the hierarchy of divergences, as shown in Figure 16, and remains independent from the diaphragm opening. In order to illustrate this property, we extracted the values of LG_{p0} divergences when Y_{PI} is equal to (0.707, 0.541, and 0.455) from Figure 16, and the results are given in Table 8. The values in red colour in Table 8 represent the minimum values of LG_{p0} beam divergence, and the minimum of losses are shown in Table 9. It now remains to be seen whether the characteristics of the fundamental mode of a plano-concave cavity, including a binary annular phase plate, simultaneously impose the p nodes of the fundamental mode, thus taking the form of LG_{p0} mode. The key parameter will mainly be the transverse mode discrimination, TMD, which is expected to be improved in comparison with the TMD obtained using a CPP (Table 11).

Table 11. Loss L_{FM} of the fundamental mode of the cavity shown in Figure A1, in which a CPP is inserted at a distance D = 5 mm from the concave mirror of radius of curvature R = 150 mm, and the diaphragm is located against the plane mirror. The fundamental mode is an LG_{p0} (p = 1, 2, and 3) depending on the normalised radius Y_{PI} of the CPP. The beam emerging from the plane mirror is characterised by its M^2 factor.

L (mm)	g	Y_{PI}	Y_c	L_{FM} in %	F_C	M^2
93	0.38	0.707	3.1	3	2.84	2.97
124	0.17	0.54	4.5	1.7	1.85	5.15
137	0.08	0.45	5	2.3	1.19	7.008

Now, let us consider the cavity shown in Figure A1 with the same parameters used in Section 2.2 when considering the multi-pass properties of absorbing rings: L = 260 mm; R = 300 mm; λ = 1064 nm; g = 0.133; W_p = 186 µm; W_c = 260 µm. The results are shown in Table 12. It can be seen that the selection of a LG_{p0} mode, as the fundamental mode with low losses, L_{FM}, is effectively carried out by inserting a BAPP#p since the M^2 factor is very close to $(2p + 1)$. It cannot be said that using a BAPP in place of a CPP inside a laser cavity significantly improves the transverse mode discrimination F_c.

Table 12. Loss L_{FM} of the fundamental mode of the cavity shown in Figure A1, in which a BAPP (see Figure 18) is inserted at a distance D = 5 mm from the concave mirror of radius of curvature R = 150 mm, and a diaphragm is located against the plane mirror. The cavity length is L = 260 mm. The fundamental mode is a LG_{p0} (p = 1, 2, and 3), depending on the BAPP inserted. The beam emerging from the plane mirror is characterised by its M^2 factor.

	Y_c	L_{FM}	F_c	M^2
BAPP#1	6.5	0.30%	2.49	3
BAPP#2	6.5	0.74%	2.88	4.98
BAPP#3	6.5	1.28%	1.59	6.97

It is important to point out that the far-field of the two cavity outputs shown in Figure A1 are characterised by distinct intensity profiles. For instance, Figure 19 displays the far-field intensity distributions, calculated in the focal plane of a converging lens, from

Out#1 and Out#2 when the BAPP#3 is inserted inside the resonator. The focused beam emerging from Out#1 is a shaped like an LG_{30}, while it is quasi-Gaussian in shape from Out#2. The latter is in fact a rectified LG_{30} beam with the same M^2 factor as the LG_{30} beam emerging from Out#1, in accordance with A.E. Siegman [60], who has demonstrated that a binary diffractive optical element is not able to improve the M^2 factor when the phase discontinuities of the BAPP correspond to the node of the incident LG_{p0} beam. In contrast, the M^2 factor is degraded if the phase discontinuities of the BAPP are shifted from the nodes of the LG_{p0} beam. This property is illustrated by the plots in Figure 20, which displays the variations in the M^2 factor of LG_{p0} beams passing through a CPP. Every time the phase discontinuity is set on a node, the M^2 factor is either unchanged or is increased. We note that the rectification of a LG_{p0} beam involves a phase object set on its path aiming to convert the alternately out-of-phase rings into a unified phase. This function is fulfilled by the BAPP#p. The rectified LG_{p0} beams have interesting properties which can be found in [21] and the references therein.

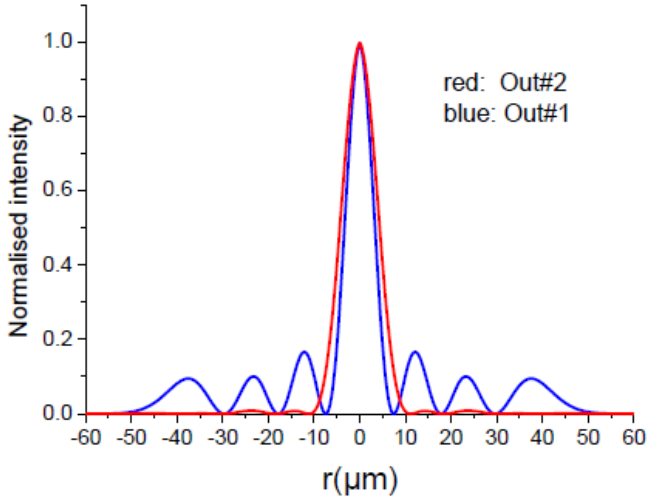

Figure 19. Intensity profile of the focused beam emerging from Out#1 and Out#2 of the cavity, including a BAPP#3. The focused beam from output Out#1 (Out#2) is an LG_{30} (quasi-Gaussian distribution).

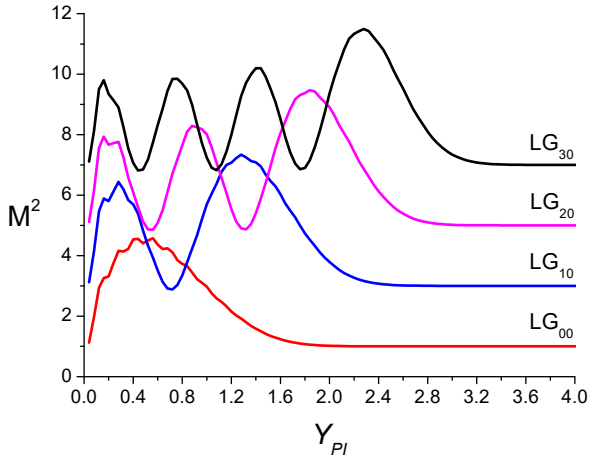

Figure 20. Variations in the M^2 factor of LG_{p0} beams (p = 0, 1, 2, and 3) passing through a CPP versus Y_{PI}.

4. Discussion

In this paper, we considered the use of binary amplitude or phase masks as intra-cavity filters for forcing the fundamental mode of a laser to be a single high-order radial Laguerre–Gauss LG_{p0} mode. The intra-cavity binary mask aims to impose the zeros of intensity of the oscillating laser beam. As soon as the nodes of the oscillating mode are imposed by the

mask, according to the positions of the zeros of the Laguerre polynomial, then the oscillating mode undergoes the lowest loss: this is a LG_{p0} mode given by Equation (1). For convenience and clarity, we limited ourselves to $p = 3$, but it may be perfectly feasible to obtain laser oscillation on higher-order transverse modes forced by a binary amplitude or phase mask.

It is important to note that the actions of the phase and amplitude masks are very different. The binary amplitude masks made up of absorbing rings induces high losses for all modes except the specific desired LG_{p0} mode. The cavity does not necessitate any supplementary clipping induced by a circular diaphragm. In this case, it was found that the transverse mode discrimination is high, provided that the rings thickness is small (10–20 μm).

The phase mask is made of a transparent material, glass for instance, on which is etched a relief which results in annular zones that introduce a phase shift equal to 0 or π, giving rise to a transmittance equal to +1 or -1. The radius of phase discontinuities ($0 \rightarrow \pi$) and ($\pi \rightarrow 0$) coincide with the zeros of intensity of the desired LG_{p0} mode. The action of the binary phase mask is the change in the divergence hierarchy of the LG_{p0} basis so that the fundamental mode selected by a diaphragm set on the other side of cavity is a single high-order LG_{p0} mode. It was found that the transverse mode discrimination obtained using the binary phase mask was lower than that obtained using a binary amplitude mask. It could be added that the fabrication of a binary phase mask is more difficult than a binary amplitude mask because of the need to control the etched quantity of glass which defines the phase shift discontinuity ($0 \rightarrow \pi$).

As was mentioned in the introduction, the LG_{p0} beams and the redressed LG_{p0} beams are characterised by a beam propagation factor $M^2 = (2p + 1)$, which disqualifies them for laser applications needing a high brightness. However, such laser beams have certain qualities which the Gaussian beam does not have [16]. In particular, a rectified LG_{p0} beam is particularly useful for improving the spatial resolution in 3D-laser prototyping [61] or the longitudinal force of optical tweezers [62]. In this context, it may be noted that the setup shown in Figure A1 has the advantage of enabling the perfect self-alignment of the binary phase mask to achieve beam rectification. This would not be the case if the beam rectification was achieved outside the laser cavity. By contrast, it is useful to note that the output Out#2 through the opaque rings (Figure A1) is a undeformed LG_{p0} beam if the intracavity beam is a LG_{p0} beam because we are dealing with zero-field occluding or non-diffracting occluding since the absorbing rings are positioned on nodes.

Since, even today, most commercial lasers utilise a Gaussian beam, there is no alternative but to build our own home laser able to deliver a LG_{p0} beam. For that, there is an important feature to consider which concerns the lateral size of the gain region in the laser medium. Indeed, this point appears when the pumping of a solid-state laser is longitudinal, since focusing the pump beam only shortly leads to an insufficient lateral extent, which is unable to sustain the laser oscillation on a high-order transverse mode with a width proportional to the mode order p.

The last point concerns power extraction, which is increased when forcing laser oscillation on a high-order transverse mode, as observed experimentally [27,38]. The interpretation of this effect is that the laser beam power is particularly proportional to the mode volume inside the cavity, which is proportional to the mode order p [27].

In this paper, we explored in detail how to force the oscillation of a laser to be present on a high-order, but single, LG_{p0}, by using a diffractive technique which consists of inserting an amplitude or a phase mask inside the resonator. It is worth noting that the use of an interferometric method is possible as a result of the pioneering experimental work accomplished by P.W. Smith [63] which was also recently modelled [64].

In the interest of completeness, the role of the active medium in the selection of the oscillating transverse mode should also be considered. In absolute terms, both the

amplifying medium and the resonator each have a contribution in transverse mode selection. However, the action of the "cold cavity", i.e., without the active medium, can be considered preponderant in cases where the pumped region of the amplifying medium is transversely much larger than the expected high-order transverse mode. This has been experimentally observed in solid-state lasers [27,36–38], and this justifies our study, which is exclusively based on the transverse properties of a "cold cavity", including binary amplitude or phase masks. Otherwise, it would be necessary to take into account the nonlinear response of the active medium, which would make the numerical determination of the transverse properties of the laser resonant field difficult.

Author Contributions: Conceptualization, K.A.-A.; methodology, K.A.-A.; software, K.A.-A. and A.H.; validation, K.A.-A., A.H. and M.F.; formal analysis, A.H., K.A.-A. and M.F.; investigation, A.H., K.A.-A. and M.F.; resources, A.H., K.A.-A. and M.F.; data curation, A.H., K.A.-A. and M.F.; writing—original draft preparation, A.H., K.A.-A. and M.F.; writing—review and editing, K.A.-A.; visualisation, A.H., K.A.-A. and M.F.; supervision, K.A.-A. All authors have read and agreed to the published version of the manuscript.

Funding: This research received no external funding.

Institutional Review Board Statement: Not applicable.

Informed Consent Statement: Not applicable.

Data Availability Statement: Data are contained within the article.

Conflicts of Interest: The authors declare no conflicts of interest.

Appendix A

We consider a plano-concave cavity made up of a plane mirror on which is set a selecting diaphragm (circular aperture) and a concave mirror, in front of which a diffractive optical element (DOE), or an absorbing ring, is placed. The DOE can be a circular phase plate (CPP) or a binary annular phase plate (BAPP). The determination of the resonator transverse mode parameters (intensity distribution, mode volume, width, etc.) is of key importance in the design of a laser system. For instance, the knowledge of the fundamental mode characteristics (M^2 factor, losses, transverse mode discrimination, etc.) are the quantities to be evaluated. For a long time, the method used for the determination of the resonant field of cavities was the so-called Fox and Li method [1] and other more or less sophisticated procedures based on integral equation solving, the solution of which is very sensitive to the initial conditions, thus giving rise to a certain amount of numerical instabilities. This is why we prefer the matrix method proposed by G. Stéphan and M. Trumper in 1983 [65], which involves, as will be shown below, a matrix operator which holds the information about amplitude and phase clipping undergone by the resonant field after insertion inside the cavity. The types of cavities that are considered in the following section are shown in Figures A1 and A2 when a phase DOE (an absorbing ring) is inserted.

Note that the binary DOE in Figure A1 is displaced from the concave mirror by a distance D, and the reason for that can be found in [35]. To understand the necessity of displacing the DOE from the mirror M_c by a distance $D << L$, we have to remember that if we consider, for instance, a DOE in form of a single-phase discontinuity or a binary annular phase plate, then the emerging beam is reshaped, since it suffers a partial or a total rectification [21]. Note that the word rectification means that the negative parts of the beam are rendered positive so that the far-field intensity distribution is no longer identical to the incident intensity distribution. If we want a LG_{p0} as the fundamental mode imposed by the binary DOE, it is important that the beam incident on the DOE, and the reflected beam by the ensemble (DOE + M_c) are together a LG_{p0} beam. For this, the reshaping effect of the

DOE, as mentioned above, must be prevented by passing the mode twice through the DOE. It is important that the distance D should be very short compared to distance L in order for the phase change introduced by the first passage to be prevented by the return passage through the DOE. In other words, if the distance D is sufficiently short then the DOE is consequently set in its own near field after reflection on the concave mirror, and as a result, the field distribution does not change.

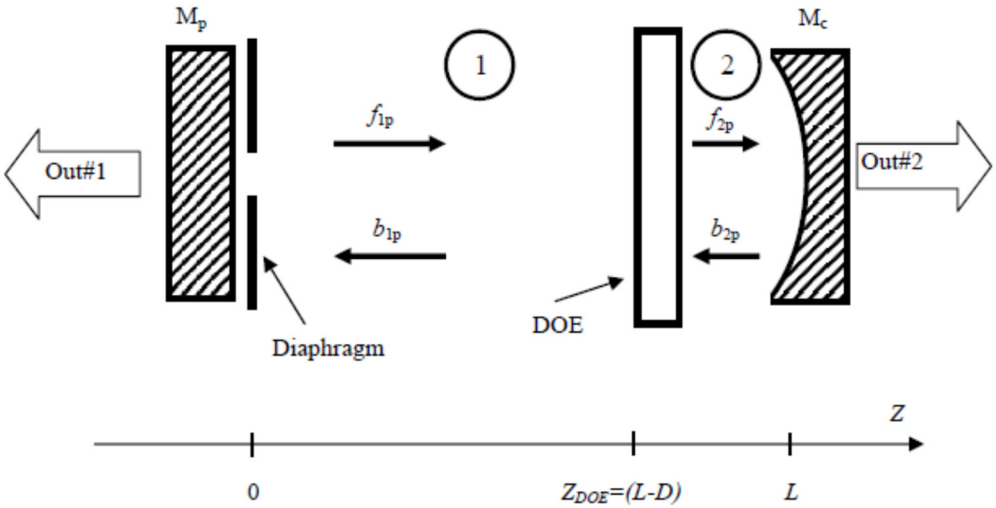

Figure A1. Description of the plano-cavity made up of a plane mirror M_p on which a diaphragm is set and a binary diffractive optical element (DOE) is inserted, which could be a CPP or a BAPP, set at a distance D = 5 mm from the concave mirror M_c with a radius of curvature R.

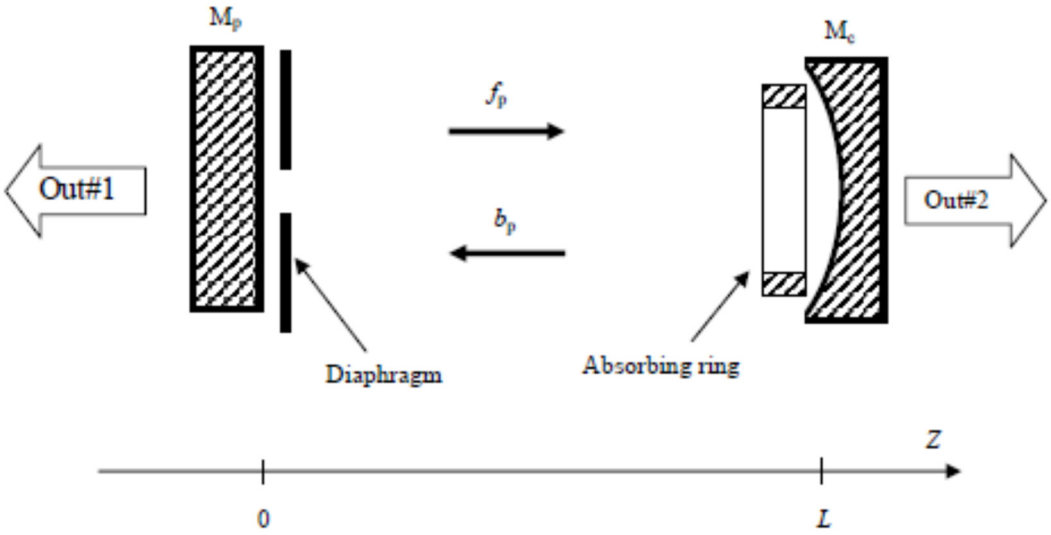

Figure A2. Apparatus showing the plano-concave cavity made up of a diaphragmed plane mirror M_p and an absorbing ring set against the concave mirror M_c.

The resonant field determination of the cavities shown in Figures A1 and A2 involves its decomposition into its two progressive waves: a forward (and backward) beam propagating in the positive (and negative) Z direction. The plane mirror position corresponds to the origin Z = 0 of the axial coordinate. The circular diaphragm set against the plane mirror has a radius labelled as ρ_C. The phase DOE (Figure A1), set at a distance D = 5 mm from the concave mirror, is characterised by its complex transmission, labelled as $\tau_{DOE}(\rho)$. The concave mirror has a radius of curvature of R = 150 mm. In Figure A2, the absorbing ring is assumed to be set against the concave mirror. The reflectivity (intensity ratio) of the plane (concave) mirror is labelled as $R_1(R_2)$.

The determination of the resonant field is carried out numerically and involves its decomposition on the basis of the eigenfunctions (eigenmodes) of the bare cavity, i.e., made up of only mirrors, M_p and M_c. Thereafter, a perfect axial symmetry is assumed for the cavity. The above mentioned eigenfunctions are formed by 80 Laguerre–Gauss functions playing the role of orthonormalised bases which, for the forward beam, are

$$G_{fp}(\rho,z) = \sqrt{\tfrac{2}{\pi}}\tfrac{1}{W(z)}L_p\left(\tfrac{2\rho^2}{W(z)^2}\right)\exp\left(-\tfrac{\rho^2}{W(z)^2}\right) \times \exp\left\{+\mathrm{i}\left[\tfrac{k\rho^2}{2R_c(z)} - (2p+1)\Phi(z)\right]\right\}, \quad \text{(A1)}$$

and for the backward beam are

$$G_{bp}(\rho,z) = \sqrt{\tfrac{2}{\pi}}\tfrac{1}{W(z)}L_p\left(\tfrac{2\rho^2}{W(z)^2}\right)\exp\left(-\tfrac{\rho^2}{W(z)^2}\right) \times \exp\left\{-\mathrm{i}\left[\tfrac{k\rho^2}{2R_c(z)} - (2p+1)\Phi(z)\right]\right\}, \quad \text{(A2)}$$

where $k = 2\pi/\lambda$. The forward and backward quantities are distinguished by the subscripts f and b, respectively. The quantities $W(z)$, $R_c(z)$, and $\Phi(z)$ are defined by Equations (2)–(4). $L_p(X)$ is the Laguerre polynomial of order p. Note that the field distribution in the bare cavity made up of mirrors M_p and M_c and is identical for the forward and backward beams. However, it has been demonstrated theoretically [66] and experimentally [35] that if there are any diffraction effects inside the resonator, then the longitudinal and transversal intensity distributions associated with the forward and backward waves are different. To facilitate the use of the following model for the determination of the resonant field of a cavity with diffracting objects, the reader may wish to refer for details to a previous work [67] on cavities with a super-Gaussian aperture or a binary circular phase plate.

(a) Cavity with a diaphragm and a binary phase mask (Figure A1):

The forward and backward fields are assumed to be linearly polarised and are expressed as linear combinations of the basic functions on both sides of the DOE:

$$E_{fj}(\rho,z) = \exp[i(kz-\omega t)]\sum_p f_{jp}G_{fp}(\rho,z), \quad \text{(A3)}$$

$$E_{bj}(\rho,z) = \exp\{i[k(2L-z)-\omega t]\}\sum_p b_{jp}G_{bp}(\rho,z). \quad \text{(A4)}$$

The index j is equal to 1 in the region 1 (by $0 < z < z_{DOE}$) and equal to 2 in the region 2 ($z_{DOE} < z < L$), where $z_{DOE} = (L - D)$ is the position of the DOE. We study the stationary field for t = 0 and then $\exp(-i\omega t)$ = 1.

The functions of the basis satisfy the orthonormalisation condition given by:

$$2\pi\int_0^\infty G_{fp}(\rho,z)G^*_{fm}(\rho,z)\rho\, d\rho = \delta_{pm} \quad \text{(A5)}$$

$$2\pi\int_0^\infty G_{bp}(\rho,z)G^*_{bm}(\rho,z)\rho\, d\rho = \delta_{pm} \quad \text{(A6)}$$

where the symbol * is used to describe the complex conjugate of the quantity. The knowledge of the forward and backward fields involves the determination of the four (ρ and z, independently) coefficients, f_{1p}, f_{2p}, b_{1p} and b_{2p}, of the field expansion for $0 < z_{DOE} < L$.

The boundary conditions at the DOE and aperture planes impose a relation between the different coefficients, and their determination involves the matrix M, known as the round-trip operator and expresses the change in the forward coefficients after a round-trip in the apertured cavity:

$$f'_{jp} = \sum_m M_{pm} f_{jm} \tag{A7}$$

The matrix M is defined by its typical element M_{lq} given by

$$M_{lq} = (R_1 R_2)^{1/2} \exp[-i2\phi_D] \sum_p C^A_{qp} \sum_n C^D_{l\,n} C^A_{np} \exp[-i4p(\Phi_D - \Phi_A)] \exp[-i(n+q)\Phi_A] \tag{A8}$$

where

$$\Phi_D = Arc\tan\left(\frac{\lambda L}{\pi W_0^2}\right) \tag{A9}$$

$$\Phi_A = Arc\tan\left(\frac{\lambda z_{DOE}}{\pi W_0^2}\right) \tag{A10}$$

$$C^A_{pm} = \int_0^\infty \tau_{DOE}(X) \exp(-X) L_p(X) L_m(X) dX \tag{A11}$$

$$C^D_{pn} = \int_0^{2Y_C^2} \exp(-Y) L_p(Y) L_m(Y) dY \tag{A12}$$

with

$$X = \frac{2\rho^2}{W^2(z_{DOE})},\ Y = \frac{2\rho^2}{{W_0}^2},\ Y_C = \frac{\rho_C}{W_0} \tag{A13}$$

The complex transmittance $\tau_{DOE}(\rho)$ associated with the binary circular phase plate, annular phase plate, and spherical aberration takes the following form:

For the circular phase plate of the radius:

$$R_{PI} :\rightarrow\ \tau_{DOE}(\rho) = \begin{cases} -1 & \text{for} \rho \le R_{PI} \\ +1 & \text{for} \rho > R_{PI} \end{cases} \tag{A14}$$

For the binary annular phase plate:

The binary annular DOE is made up of annular zones introducing a phase shift equal to 0 or π, giving rise to a transmittance given by Equation (A15):

$$\tau_{DOE}(\rho) = \begin{cases} -1 & \text{for } 0 < \rho \le \rho_1 \\ (-1)^{i+1} & \text{for } \rho_i < \rho \le \rho_{i+1} \text{ and } (i+1) < p \\ (-1)^{p+1} & \text{for } \rho > \rho_p \end{cases} \tag{A15}$$

The position of the phase jumps from 0 to π or π to 0, exactly following the zeros of the Laguerre polynomial L_p given in Table 1, where ρ_i's are the p radial positions for which the intensity of the desired LG_{p0} mode is zero.

It is important to note that the round-trip operator M contains the information about reflection at the mirrors and about amplitude (phase) clipping at the edge of the diaphragm (DOE). The resonance condition is expressed by the relation $f'_{jp} = \Gamma f_{jp}$ which holds for all

p after a round-trip. This allows us to consider the eigenmodes of the phase/amplitude apertured cavity as the eigenvectors u of the matrix M, defined as

$$Mu = \Gamma u. \tag{A16}$$

where Γ is the complex eigenvalue associated with the eigenvector u. A remarkable eigenvector is that which has the largest eigenvalue, labelled $|\Gamma_{FM}|$, thus defining the fundamental mode of the cavity whose power loss per round-trip is given by

$$L_{FM} = 1 - |\Gamma_{FM}|^2 \tag{A17}$$

The second eigenvector of M has the second greatest eigenvalue, labelled as $|\Gamma_{SEC}|$, and is the second transverse mode whose power loss per round-trip is given by

$$L_{SEC} = 1 - |\Gamma_{SEC}|^2 \tag{A18}$$

From a practical point of view, the cavity with an amplifying medium constitutes a laser which, at the threshold, will oscillate first on the above-mentioned fundamental mode since it has the lowest losses. From this step, increasing the pumping action will lead to the emergence of a second transverse mode.

In order for the laser to be able to oscillate on the desired fundamental mode, which could be a high-order transverse LG_{p0} mode before the second transverse mode begins the oscillation, the difference between L_{FM} and L_{SEC} must be as large as possible. This possibility of a cavity to contain a second transverse mode can be described by a transverse mode discrimination factor, defined as

$$F_c = L_{SEC}/L_{FM} \tag{A19}$$

(b) Cavity with a diaphragm and an absorbing ring (Figure A2):

In this case, as shown in Figure A2, the determination of the resonant field requires knowledge of only two coefficients, f_p's and b_p's. As previously, the change in the forward coefficients after a round-trip in a cavity with a diaphragm on the plane mirror, and an absorbing ring can be described by Equation (A7), but the typical element M_{pm} is given by

$$M_{pm} = (R_1 R_2)^{1/2} \sum_n C^D_{pn}.C^R_{nm} \exp[-2i(n+m+1)\Phi_D] \tag{A20}$$

where

$$C^R_{nm} = \int_0^{2Y_A^2} \exp(-G) L_p(G) L_m(G) dG + \int_{2Y_B^2}^{\infty} \exp(-G) L_p(G) L_m(G) dG \tag{A21}$$

and

$$G = \frac{2\rho^2}{W^2(L)},\ Y_A = \frac{\rho_A}{W(L)},\ Y_B = \frac{\rho_B}{W(L)}. \tag{A22}$$

The numerical computation of overlapping integrals C^A_{pm}, C^D_{pn}, and C^R_{nm} is carried out using a double precision FORTRAN 77 routine based on the integration subroutine *DQDAG* from IMSL. The numerical calculation of the eigenvectors and eigenvalues of the complex matrix M is carried out using the double precision routine *DEVCCG*. The compiler used is from the ABSOFT company.

(c) Output beam

The cavities shown in Figures A1 and A2 have two outputs whose intensity profiles are not necessarily identical, especially in the case of Figure A1, considering the ability of the phase DOE to achieve a beam reshaping [21]. Like the forward and backward fields, the field $E_1(\rho,z)(E_2(\rho,z))$, associated with the beam emerging from the output#1 (#2), is developed on the basis of the Laguerre–Gauss functions:

$$E_1(\rho,z) = \sum_p D_{1,p} G_{bp}(\rho,z) \tag{A23}$$

$$E_2(\rho,z) = \sum_p D_{2,p} G_{fp}(\rho,z) \tag{A24}$$

The coefficients of expansion $D_{1,p}$ ($D_{2,p}$) of the laser output field $E_1(\rho,z)(E_2(\rho,z))$ emerging from the output#1 (output#2) can be expressed as a function of the internal coefficients b_p or b_{1p} (f_{2p}), according to the method already used in [67]. If one knows the coefficients of D_p, labelled as $D_{1,p}$ and $D_{2,p}$, it is easy to deduce the M^2 factor of the beam emerging from output #1 or #2 as follows [68]:

$$M^2 = \left[\left\{ \sum_p (2p+1)\left|D_p\right|^2 \right\}^2 - 4\left\{ \sum_p \sum_q p(D_p^* D_q)^r \delta_{p,q+1} \right\}^2 \right]^{1/2} \tag{A25}$$

where the superscript r is used to describe the real part of the quantity.

References

1. Fox, A.G.; Li, T. Resonant modes in a maser interferometer. *Bell Syst. Tech. J.* **1961**, *40*, 453–488. [CrossRef]
2. Boyd, G.D.; Gordon, J.P. Confocal multimode resonator for millimetre through optical wavelength masers. *Bell Syst. Tech. J.* **1961**, *40*, 489–508. [CrossRef]
3. Boyd, G.D.; Kogelnik, H. Generalized confocal resonator theory. *Bell Syst. Tech. J.* **1962**, *41*, 1347–1369. [CrossRef]
4. Li, T. Diffraction loss and selection of modes in maser resonators with circular mirrors. *Bell Syst. Tech. J.* **1965**, *44*, 917–931. [CrossRef]
5. Kogelnik, H.; Li, T. Laser beams and resonators. *Appl. Opt.* **1966**, *5*, 1550–1567. [CrossRef]
6. Fox, A.G.; Li, T. Computation of resonator modes by the method of resonant excitation. *IEEE J. Quantum Electron.* **1968**, *4*, 460–465. [CrossRef]
7. Valle, A. Selection and modulation of high-order transverse modes in vertical-cavity surface-emitting lasers. *IEEE J. Quantum Electron.* **1998**, *34*, 1924–1932. [CrossRef]
8. Quirce, A.; Valle, A.; Hurtado, A.; Gimenez, C.; Pesquera, L.; Adams, M.J. Experimental study of transverse mode selection in VCSELs induced by parallel polarised optical injection. *IEEE J. Quantum Electron.* **2010**, *46*, 467–473. [CrossRef]
9. Kim, K.; Bittner, S.; Zeng, Y.; Guazzotti, S.; Hess, O.; Wang, Q.J.; Cao, H. Massively parallel ultrafast random bit generation with a chip-scale laser. *Sciences* **2021**, *371*, 948. [CrossRef]
10. Kim, K.; Bittner, S.; Zeng, Y.; Guazzotti, S.; Hess, O.; Wang, Q.J.; Cao, H. Sensitive control of broad-area semiconductor lasers by cavity shape. *APL Photonics* **2022**, *7*, 056106. [CrossRef]
11. Ledentsov, N.N.; Makarov, Y.; Shchukin, V.A.; Kalosha, V.P.; Leventsov Jr, N.; Chrochos, L.; Bou Sanayeh, M.; Turkiewicz, J.P. High speed VCEL Technology and applications. *J. Light Technol.* **2022**, *40*, 1749–1763. [CrossRef]
12. Koechner, W. *Solid-State Laser Engineering*, 6th ed.; Springer Sciences: Berlin/Heidelberg, Germany, 2006.
13. Saleh, B.E.A.; Teich, M.C. *Fundamentals of Photonics*, 2nd ed.; Wiley-Interscience: Hoboken, NJ, USA, 2007.
14. Hodgson, N.; Weber, H. *Laser Resonators and Beam Propagation*, 2nd ed.; Springer Sciences: Berlin/Heidelberg, Germany, 2005.
15. Arfken, G. *Mathematical Methods for Physicists*, 2nd ed.; Academic Press: Cambridge, MA, USA, 1973.
16. Menzel, R. *Photonics*; Springer: Cham, Switzerland, 2001; Chapter 2.
17. Aït-Ameur, K. Amplitude and phase clipping: Strehl ratio versus divergence. *Opt. Commun.* **2012**, *285*, 699–705. [CrossRef]
18. Siegman, A.E. New developments in laser resonators. *Proc. SPIE* **1990**, *1224*, 2–14.
19. Johnston, T.F. M^2 concept characterizes beam quality. *Laser Focus World* **1990**, *26*, 173–174.
20. Siegman, A.E. Defining, measuring, and optimizing laser beam quality. *Opt. Reson. Coherent Opt.* **1993**, *1868*, 2–14.
21. Ait-Ameur, K. The Advantages and Disadvantages of Using Structured High-Order but Single Laguerre–Gauss LG_{p0} Laser Beams. *Photonics* **2024**, *11*, 217. [CrossRef]

22. Chelkowski, S.; Hild, S.; Freise, A. Prospects of higher-order Laguerre-Gauss modes in future gravitational wave detectors. *Phys. Rev. D* **2009**, *79*, 122002. [CrossRef]
23. Granata, M.; Buy, C.; Ward, R.; Barsuglia, M. Higher-order Laguerre-Gauss mode generation and interferometry for gravitational wave detectors. *Phys. Rev. Lett.* **2010**, *105*, 231102. [CrossRef]
24. Sorazu, B.; Fulda, P.J.; Barr, B.W.; Bell, A.S.; Bond, C.; Carbone, L.; Freise, A.; Hild, S.; Huttner, S.H.; Macarthur, J.; et al. Experimental test of higher-order Laguerre-Gauss modes in the 10 m Glasgow prototype interferometer. *Class. Quantum Grav.* **2013**, *30*, 035004. [CrossRef]
25. Alloca, A.; Gatto, A.; Tacca, M.; Day, R.A.; Barsuglia, M.; Pillant, G.; Buy, C.; Vajente, G. Higher-order Laguerre-Gauss interferometry for gravitational wave detectors with in situ mirror defects compensation. *Phys. Rev. D* **2015**, *92*, 102002. [CrossRef]
26. Noack, A.; Boyan, C.; Willke, B. Higher-order Laguerre-Gauss modes in (non-) planar four-mirror cavities for future gravitational wave detectors. *Opt. Lett.* **2017**, *42*, 751–754. [CrossRef] [PubMed]
27. Ngcobo, S.; Aït-Ameur, K.; Passilly, N.; Hasnaoui, A.; Forbes, A. Exciting higher-order radial Laguerre-Gaussian modes in a diode-pumped solid-state laser resonator. *Appl. Opt.* **2013**, *52*, 2093–2101. [CrossRef] [PubMed]
28. Abramski, K.M.; Baker, H.J.; Colley, A.D.; Hall, D.R. Single mode selection using coherent imaging within a slab waveguide CO_2 laser. *Appl. Phys. Lett.* **1992**, *60*, 2469–2471. [CrossRef]
29. Chu, S.C.; Chen, Y.T.; Tsai, K.F.; Otsuka, K. Generation of high-order Hermite-Gaussian modes in end-pumped solid-state lasers for square vortex array laser beam generation. *Opt. Express* **2012**, *20*, 7128–7141. [CrossRef]
30. Smith, P.W. Mode selection in Lasers. *Proc. IEEE* **1965**, *60*, 422–440. [CrossRef]
31. Gordon, J.P.; Kogelnik, H. Equivalence relations among spherical mirror optical resonators. *Bell Syst. Tech. J.* **1964**, *43*, 2873–2886. [CrossRef]
32. Li, T. Mode selection in an aperture-limited concentric maser interferometer. *Bell Syst. Tech. J.* **1963**, *42*, 2609–2620. [CrossRef]
33. Kortz, H.P.; Weber, H. Diffraction losses and mode structure of equivalent TEM_{00} optical resonators. *Appl. Opt.* **1981**, *20*, 1936–1940. [CrossRef]
34. Cagniot, E.; Derrar-Kaddour, Z.; Fromager, M.; Aït-Ameur, K. Improving both transverse mode discrimination and diffraction losses in a plano-concave cavity. *Opt. Commun.* **2008**, *281*, 4449–4454. [CrossRef]
35. Naidoo, D.; Ait-Ameur, K.; Litvin, I.; Fromager, M.; Forbes, A. Observing mode propagation inside a laser cavity. *New J. Phys.* **2012**, *14*, 053021. [CrossRef]
36. Oron, R.; Danziger, Y.; Davidson, N.; Friesem, A.A.; Hasman, E. Discontinuous phase elements for transverse mode selection in laser resonators. *Appl. Phys. Lett.* **1999**, *74*, 1373–1375. [CrossRef]
37. Ishaaya, A.A.; Davidson, N.; Machavariani, G.; Hasman, E.; Friesem, A.A. Efficient selection of High-order Laguerre-Gaussian modes in a Q-switched Nd:YAG laser. *IEEE J. Quantum Electron.* **2003**, *9*, 74–82. [CrossRef]
38. Ishaaya, A.A.; Davidson, N.; Machavariani, G.; Hasman, E.; Friesem, A.A. Very high-order pure Laguerre-Gaussian mode selection in a passive Q-switched Nd:YAG laser. *Opt. Express* **2005**, *13*, 4952–4962. [CrossRef] [PubMed]
39. Senatsky, Y.; Bisson, J.F.; Shelobolin, A.; Shirakawa, A.; Ueda, K. Circular modes selection in Yb:YAG laser using an intracavity lens with spherical aberration. *Laser Phys.* **2009**, *19*, 911–918. [CrossRef]
40. Thirugnansambandam, M.P.; Senatsky, Y.; Ueda, K. Generation of very-high order Laguerre-Gaussian modes in Yb:YAG ceramic laser. *Laser Phys. Lett.* **2010**, *7*, 637–643. [CrossRef]
41. Senatsky, Y.; Bisson, J.F.; Shirakawa, A.; Thirugnansambandam, M. Laguerre-Gaussian modes selection in diode-pumped solid-state lasers. *Opt. Rev.* **2012**, *19*, 201–222. [CrossRef]
42. Sheng, Q.; Wang, A.; Ma, Y.; Wang, S.; Wang, M.; Shi, Z.; Liu, J.; Fu, S.; Shi, W.; Yao, J.; et al. Intracavity spherical aberration for selective generation of single-transverse-mode Laguerre-Gaussian output with order up to 95. *PhotoniX* **2022**, *3*, 4. [CrossRef]
43. Hall, D.R.; Jackson, P.E. *The Physics and Technology of Laser Resonators*; Institute of Physics Publishing: Bristol, UK, 1992; Chapter 9.
44. Ait-Ameur, K. Influence of the longitudinal position of an aperture inside a cavity on the transverse mode discrimination. *Appl. Opt.* **1993**, *32*, 7366–7372. [CrossRef]
45. Mudge, D.; Ostermeyer, M.; Veitch, P.J.; Munch, J.; Middlemiss, B.; Ottaway, D.J.; Hamilton, M.W. Power scalable TEM_{00} CW Nd:YAG laser with thermal lens compensation. *IEEE J. Sel. Top. Quantum Electron.* **2000**, *6*, 643–649. [CrossRef]
46. Graf, T.; Wyss, E.; Roth, M.; Weber, H.P. Laser resonator with balanced thermal lenses. *Opt. Commun.* **2000**, *190*, 327–331. [CrossRef]
47. Wyss, E.; Roth, M.; Graf, T.; Weber, H.P. Thermooptical compensation methods for high-power lasers. *IEEE J. Quantum Electron.* **2002**, *38*, 1620–1628. [CrossRef]
48. Chen, H.; Liu, Q.; Yan, X.; Gong, M. High power Q-switched TEM_{00} Nd:YVO_4 laser self-adaptive compensation of thermal lensing effect. *Las. Phys.* **2010**, *20*, 1594–1597. [CrossRef]
49. Wang, J.; Cheng, T.; Wang, L.; Yang, J.; Sun, D.; Yin, S.; Wu, X.; Jiang, H. Compensation of strong thermal lensing in an LD side-pumped high-power Er: YSGG laser. *Las. Phys.* **2015**, *12*, 105004. [CrossRef]

50. Shang, P.; Bai, L.; Wang, S.; Cai, D.; Li, B. Research progress on thermal effect of LD pumped solide state laser. *Opt. Las. Eng.* **2023**, *157*, 108640.
51. Veldkamp, W.B.; McHugh, T.J. Binary optics. *Sci. Am.* **1992**, *266*, 92–97. [CrossRef]
52. O'Shea, D.C.; Beletic, J.W.; Poutous, M. Binary-mask generation for diffractive optical elements using microcomputers. *Appl. Opt.* **1993**, *32*, 2566–2572. [CrossRef]
53. Cordingley, J. Application of a binary diffractive optics for beam shaping in semiconductor processing by lasers. *Appl. Opt.* **1993**, *32*, 2538–2542. [CrossRef]
54. Skeren, M.; Ritcher, I.; Fiala, P. Design of binary phase-only diffractive optical elements for laser beam shaping. *Proc. SPIE Laser Beam Shap.* **2000**, *4095*, 154–164.
55. Raciukaitis, G.; Stankevicius, E.; Geys, P.; Gedvilas, M.; Bischoff, C.; Jäger, E.; Umhofer, U.; Völklein, F. Laser processing by using diffractive optical laser beam shaping technique. *J. Laser Micro/Nanoeng.* **2011**, *6*, 37–43. [CrossRef]
56. Siemon, A.; Siemon, A.; Suszek, J.; Kowalczyk, A.; Bomba, J.; Sobczyk, A. THz beam shaping based on paper diffractive optics. *IEEE Trans. Terahertz Sci. Technol.* **2016**, *6*, 568–575. [CrossRef]
57. Barlev, O.; Golub, M.A. Multifonctional binary diffractive optical elements for structured light projectors. *Opt. Express* **2018**, *26*, 21092–21107. [CrossRef] [PubMed]
58. Marchesini, S.; Sakdinawat, A. Shaping coherent x-rays with binary optics. *Opt. Express* **2019**, *27*, 907–917. [CrossRef] [PubMed]
59. Cagniot, E.; Fromager, M.; Godin, T.; Passilly, N.; Brunel, M.; Ait-Ameur, K. Variant of the method of Fox and Li dedicated to intracavity laser beam shaping. *J. Opt. Soc. Am. A* **2011**, *28*, 489–495. [CrossRef]
60. Siegman, A.E. Binary phase plates cannot improve laser beam quality. *Opt. Lett.* **1993**, *18*, 675–677. [CrossRef]
61. Hasnaoui, A.; Bencheikh, A.; Aït-Ameur, K. Tailored TEM_{p0} beams for large size 3-D laser prototyping. *Opt. Las. Eng.* **2011**, *49*, 248–251. [CrossRef]
62. Haddadi, S.; Ait-Ameur, K. Improvement of optical trapping effect by structuring the illuminating laser beam. *Optik* **2022**, *251*, 168439. [CrossRef]
63. Smith, P.W. Stabilised single-frequency output from a long laser cavity. *IEEE J. Quantum Electron* **1965**, *1*, 343–348. [CrossRef]
64. Habchi, A.; Harfouche, A.; Aït-Ameur, K. Flexible control of laser transverse modes using a Fox-Smith mirror. *Appl. Phys. B* **2021**, *127*, 97. [CrossRef]
65. Stéphan, G.; Trümper, M. Inhomogeneity effects in a gas laser. *Phys. Rev. A.* **1983**, *28*, 2344–2362. [CrossRef]
66. Ait-Ameur, K.; Ladjouze, H. Fundamental mode distribution in a diaphragmed cavity. *J. Phys. D Appl. Phys.* **1988**, *21*, 1566–1577. [CrossRef]
67. De Saint Denis, R.; Passilly, N.; Aït-Ameur, K. Laser beam brightness of apertured resonators. *Opt. Commun.* **2006**, *264*, 193–202. [CrossRef]
68. Vicalvi, S.; Borghi, R.; Santarsiero, M.; Gori, F. Shape-invariance error for axially symmetric light beams. *J. Quantum Electron.* **1998**, *34*, 2109–2116. [CrossRef]